Shapes and Genescapes: Mapping Multivariate Phenotype-Biological Process Associations for Craniofacial Shape

November 12, 2020

J. David Aponte[1], David C. Katz[1], Wei Liu[1], Fernando Andrade[2], Charles C. Roseman[3], Stephen A. Murray[4], James Cheverud[2], Ralph S. Marcucio[5], Benedikt Hallgrímsson[1*]

1) Department of Cell Biology & Anatomy, Alberta Children's Hospital Research Institute and McCaig Bone and Joint Institute, Cumming School of Medicine, University of Calgary, AB, Canada

2) Department of Biology, Loyola University Chicago, Chicago, IL, USA

3) Department of Animal Biology, University of Illinois Urbana Champaign, Urbana, IL, USA

4) The Jackson Laboratory, Bar Harbor, ME, USA

5) Department of Orthopaedic Surgery, School of Medicine, University of California San Francisco, San Francisco, CA, USA

* Correspondence to bhallgri@ucalgary.ca

Abstract

The importance of coordinated gene effects on morphological phenotypes is clear from the intertwining of gene actions in signaling pathways, gene regulatory networks, and developmental processes underlying the development of shape and size. However, genome wide association studies identify and localize the contribution of individual genes to phenotypic variation, seldom targeting the coordinated influence of multiple genes on phenotypes. Here, we explicitly model the joint effect of biologically coherent collections of genes on craniofacial shape in a sample of n = 1,145 mice from the Diversity Outbred (DO) experimental line. We use biological process gene ontology (GO) annotations to select skeletal and facial development gene sets and solve for the axis of shape variation that maximally covaries with gene set marker variation. Our process-centered view of cranial shape variation allows us to consider fundamental issues that are difficult to address with existing methods, such as the extent to which variation in different processes relevant to the same phenotype correspond to similar axes of shape variation, and whether the direction of the effect of experimental mutations to a pathway gene is similar to the primary axis of shape variation associated with that pathway. Finally, we introduce an online application which provides users the means to customize their own process-centered craniofacial shape analyses in the DO. The process-centered approach is generally applicable to any continuously varying phenotype and thus has wide-reaching implications for complex-trait genetics.

Keywords: multivariate genotype-phenotype map, complex traits, mouse, craniofacial, diversity outbred

Introduction

Variation in human craniofacial shape is moderately to highly heritable (~30-70% (Cole et al., 2017; Tsagkrasoulis et al., 2017)), and resemblances among close relatives as well as twins underscore the strong relationship between shared genetics and shared phenotype (Johannsdottir et al., 2005; Nakata, 1985). Despite many studies in humans and in mice (Claes et al., 2018; Cole et al., 2016; Shaffer et al., 2016), we know very little about the genetic basis for variation in craniofacial shape. This is likely due to genetic complexity (Katz et al., 2019; Richtsmeier and Flaherty, 2013; Visscher, 2008; Wood et al., 2014; Wray et al., 2013). Like many aspects of morphological variation, craniofacial shape is extraordinarily polygenic. Genes with major mechanistic roles in facial development such as *Fgf8* often contribute little to standing phenotypic variation (Green et al., 2017) while genetic influences without obvious connections to craniofacial development emerge as significant contributors (Kenney-Hunt et al., 2008; Klingenberg and Leamy, 2001; Maga et al., 2015; Pallares et al., 2015, 2014). The effects of genetic variants on phenotype often depend on genetic background (Mackay and Moore, 2014; Percival et al., 2017) and many mutations have variably penetrant effects even when background is controlled (Hallgrimsson et al, 2009; Rendel, 1967). These issues likely arise because genetic influences act through multiple layers of interacting developmental processes to influence phenotypic traits, resulting in complex patterns of epistasis and variance heterogeneity (Hallgrimsson et al., 2018, 2014; Kawauchi et al., 2009; Wagner and Zhang, 2011). Solutions that go beyond studies of single gene effects are required to overcome these significant challenges in complex-trait genetics. Here, we implement an enhanced form of the more general candidate gene approach to evaluate the conjoint effects of multiple genes on a complex trait – craniofacial shape.

There are two basic approaches to mapping genetic effects on to phenotypic variation. A candidate gene approach measures genotypic values with known physiological and biochemical relationships to the phenotypes of interest (Cheverud and Routman, 1993). In contrast, a random marker or genome-wide approach seeks to associate any potential genetic variant with variation in the trait of interest. There are advantages and disadvantages to these two approaches. The candidate gene approach is blind to the unknown – phenotypic variation is often associated with genes not expected to be important. On the other hand, a candidate gene approach allows direct

measurement of genotypic values and produces results that are interpretable in terms of trait physiology or development. A genome-wide or random marker approach can produce unexpected insight by revealing novel gene-phenotype associations. However, this comes at a great cost in power (Visscher et al., 2017). For highly polygenic traits, this approach often produces a "tip of the iceberg" effect in which studies reveal a small and often incoherent subset of the genes that actually determine variation in the trait of interest (Broman and Sen, 2009, p. 123-124).

Several strategies have been developed that partially overcome these tradeoffs. One solution is the use of polygenic risk scores. Polygenic risk scores assess the overall genetic influence on a trait without regard to the genome-wide significance of individual SNP effects (Dudbridge, 2013; Wray et al., 2007). Approaches such as meta-analyses of genome-wide association studies (GWAS) or studies based on extreme phenotypes (Morozova et al., 2015) have expanded gene lists for a variety of complex traits. However, lengthy lists of genes or overall genomic risk for specific phenotypes do not necessarily constitute tractable genetic explanations for phenotypic variation. When 1000s of genes are required to explain heritable variation in stature, for instance, it is not clear what such lists tell you beyond the obvious fact that stature is heritable and polygenic (Yang et al., 2010; Wood et al., 2014). This tension between hypothesis-driven and hypothesis-free approaches and their attendant tradeoffs between statistical power and interpretability is, arguably, a major issue within complex trait genetics. To resolve this conceptual conflict, approaches are needed that integrate quantitative genetics with biological insights regarding the cellular and developmental processes through which genes influence phenotypic variation.

Building on Mitterocker *et al.'s* (2016) multivariate genotype-phenotype (MGP) method, we extend the candidate-gene framework to evaluate the combined contributions of genes that share ontological information such as membership in pathways that influence craniofacial development in mice. Our process-centered, multivariate approach brings traditional GWAS together with a simplified model of the hierarchical genotype-phenotype (GP) map. GP maps describe the relationship between genetic and phenotypic measurements (Lewontin, 1974). Understanding the genetic determinants of craniofacial variation, as with most complex traits, represents a many-to-

many GP map problem (Fig 1). Both phenotypic and genotypic measurements have complex within-set covariance structures. On the genetic side, the covariance structure is represented by pathway/biochemical interactions, as well as chromosomal structure like linkage, chromatin, and 3D chromosomal organization. For shape-related phenotypes, the covariance matrix is structured by the chosen set of landmarks and their resulting coordinates. The functional relationship from genotype to phenotype is then described by a between-set covariance (Klingenberg and Leamy, 2001; Mitteroecker et al., 2016). To dissect these relationships, we use a regularized partial least squares (PLS) (Lorenzo et al., 2019) approach to estimate a low-dimensional mapping from the alleles in our sample to variation in adult mouse craniofacial shape. We focus on how allelic variation in processes relevant to craniofacial development maps to craniofacial shape variation. To do so, we estimate the joint effects on multivariate craniofacial variation of markers for groups of genes that share functionally relevant gene ontology terms. We ask the following four questions:

1) How much shape variation is communally accounted for by genes contributing to a process, e.g., chondrocyte differentiation?
2) How similar are the effects of different processes on shape? For instance, do cell proliferation genes affect face shape in a similar way to genes in the bone morphogenic protein pathway?
3) How similar are mutant model effects and process effects? For example, do chondrocyte mutant effects align with the effects of natural variants in chondrocyte differentiation genes?
4) What is the overarching structure of process effects? Do process effects align with major axes of variation or other interesting directions in morphospace?

158 **Results**

159

160 **Process Multivariate Genotype-Phenotype (MGP) Mapping**

161

162 We demonstrate regularized-PLS MGP mapping with two examples. The first estimates the
163 primary axis of skull shape covariation with genes involved in chondrocyte differentiation (Fig
164 2). Differentiation of chondrocytes is one of several key developmental milestones involved in
165 endochondral ossification. Endochondral bones form the majority of the cranial base through a
166 cartilage model of bone formation (Percival and Richtsmeier, 2013). There are 38 genes
167 annotated to chondrocyte differentiation in the Ensembl database (Yates et al., 2020). Genetic
168 effects are shown as zero-centered bars that span the range of estimated allele effects across the 8
169 DO founders; individual founder allele effects—8 per marker—are color-coded within those bars
170 (Fig 2A). Among chondrocyte differentiation genes, *Nov*, *Mapk14*, and *Bmpr1b* (*Alk6*) most
171 heavily drive covariation with craniofacial shape. The phenotypic effects at each landmark—
172 magnified 4x— primarily relate to antero-posterior positioning of the zygomatic arches and
173 dorso-ventral jugal position (Fig 2B, 2C). The chondrocyte differentiation GP map explains
174 2.15% of the total variance in craniofacial shape. Compared to 1000 randomly generated marker
175 sets of the same size (38), chondrocyte differentiation explains substantially more variation in
176 phenotype than random markers (Supp fig 1A).

177

178 Figure 2B and 2C also compare the direction of the chondrocyte differentiation MGP axis
179 to the axis of shape variation of a relevant mutant phenotype. We chose homozygous *Bmpr1b*
180 mutants for this comparison because Bmpr1b heterodimerization with other bone morphogenic
181 protein pathway receptors is essential for chondrocyte differentiation and proliferation (Liu et al.,
182 2005; Yoon et al., 2005). The overall phenotypic directions of *Bmpr1b* mutant variation and
183 chondrocyte differentiation variation are moderately correlated at r = 0.312, but the direction at
184 landmarks with large effects in mutant and MGP are clearly coincident. Over the landmarks we
185 measured, the chondrocyte differentiation effect is less global than the *Bmpr1b* effect, likely due
186 to the difference in severity of the mutant phenotype.

187

188 The second example quantifies shape associations with the 41 genes annotated to
189 fibroblast growth factor (FGF) receptor signaling. The FGF pathway contributes to several
190 aspects of craniofacial development, from the epithelial to mesenchymal transition of neural
191 crest cell precursors in early facial formation, to the outgrowth of the later facial prominences
192 and specification of intramembranous and endochondral bone (Jin et al., 2012; Ornitz and Marie,
193 2015; Richman et al., 1997). Alleles from the WSB founder background for *Fgf2* and *Flrt2*
194 contribute the most variance to the phenotypic effect (Fig 3C), primarily the relative proportions
195 of vault and face (Fig 3A, 3B). The phenotype associated the *Fgfr* alleles is predominately
196 related to a larger neurocranium volume relative to the outgrowth of the face. FGFR signaling
197 loci explain 1.4% of the total variance in craniofacial shape, which greatly exceeds 1000
198 randomly selected marker sets of the same size (Supp fig 1B).
199
200 Finally, we compared the estimated FGF signaling MGP effect with the direction of an
201 *Fgf10* homozygous mutant. FGF10 is a key ligand in early development, directing proliferation
202 as well as differentiation for many craniofacial components, including the palate, teeth, and
203 bones (Hilliard et al., 2005; Prochazkova et al., 2018; Watson and Francavilla, 2018). The vector
204 correlation between the FGF mutant and the estimated FGF signaling effect is 0.623. Both
205 phenotypes strongly affect the cranial base, and the vector correlation between base landmarks is
206 0.94.
207
208 In all, we have shown how sets of allelic variation in the genome can map to distinct
209 phenotypic directions. Each MGP model shows the relative contributions of different genotypes
210 for craniofacial variation. For both examples, we focus only on the first PLS axis, so other alleles
211 for other genes may contribute to novel phenotypic directions in lower PLS axes. In both cases,
212 we were able to find mouse mutant phenotypes with moderate to strongly correlated craniofacial
213 phenotypes. In the next sections we will examine how MGP phenotypes relate to each other, as
214 well as the phenotypic directions of many mutant mouse models.
215
216 **Pairwise comparison of craniofacial development processes**
217

We chose 15 processes integral to craniofacial development and compared the pairwise similarity of effect on craniofacial shape using a heatmap based on clustering of the correlation matrix (R Core Team, 2020). Processes with similar effects on craniofacial shape will be highly correlated, while processes that affect distinct aspects of craniofacial variation will be uncorrelated to each other. The clustering algorithm resulted in two main blocks of strongly correlated effects (Fig 4A). The largest block of highly correlated phenotypic effects includes neural crest cell migration, epithelial to mesenchymal transition, forebrain development, as well as some of the most general developmental processes like cell proliferation, bone development, apoptosis, A/P pattern specification, and FGFR signaling. In addition, there is a general BMP block, with Bmp signaling, dorsoventral pattern formation, endochondral ossification, and positive regulation of skeletal muscle tissue growth. Interestingly, phenotypic variation associated with cranial suture morphogenesis, neural tube patterning, and intramembranous ossification is largely uncorrelated with the other craniofacial developmental processes included here.

To assess the stability of the clustering result, we estimated the vector correlation between the cluster distances—also known as the cophenetic distance— and the original correlation matrix. A high vector correlation suggests reliable clustering, whereas a low correlation suggests a random clustering result. The correlation between the cophenetic distance matrix and the correlation matrix is 0.648 ($t = 8.64$, $df = 103$, $p = 7.6^{-14}$), suggesting a moderate, though significant structure in the similarity of effects amongst this set of MGP processes.

Comparison of processes to principal component directions

Almost a third of the 15 pairwise process comparisons showed a vector correlation > 0.5, suggesting that many processes may feed into a limited set of directions in morphospace. To assess the extent to which different processes affect the same aspects of facial shape we randomly chose 1,000 process annotations, fit individual regularized PLS models to each set of markers for a given annotation term, and then compared the direction of phenotypic effects for each model to principal components 1-4 of the DO shape data (Fig 4B). Doing so with principal components allows us to highlight similarities in directions of process effects. Process effects

249 range from completely uncorrelated to PC1 to highly correlated (0.0 - 0.8). However, the central
250 tendency of randomly selected process effects is one of moderate-to-high correlation with PC1.
251 Moderate correlations (0.55 - 0.6) with PC1 are more common than uncorrelated effects.
252 Supplemental table 1 contains the 10 most highly correlated processes with PC1 as well as the
253 corresponding correlations to PC 2-4. The most highly correlated process to PC1 is "zinc ion
254 binding", which is 0.86 correlated to the PC1 direction. The remaining 9 processes most highly
255 correlated to PC1 includes "sensory perception of sound", "Calcium ion transport", "Protein
256 homooligomerization", "Dendrite morphogenesis", "Neuropeptide signaling pathway", "Focal
257 adhesion", "Chromosome segregation", "Sarcomere organization", and "Integral component of
258 endoplasmic reticulum membrane".
259
260 Process correlations with PCs 2-4 are generally less strong. The maximum correlated
261 process with PCs 2-4 was "V(D)J recombination", "n-terminal protein myristoylation", and
262 "branching morphogenesis of an epithelial tube" with vector correlations of 0.72, 0.89, and 0.56,
263 respectively. Processes with high vector correlations for a given PC tend to be uncorrelated with
264 other PCs (Supp table 1), although some processes load moderately high across several PCs. For
265 example, "negative regulation of I-kappaB kinase/NF-kappaB signaling" shows vector
266 correlations between 0.25 - 0.54 for the first four PCs (Supp table 2).
267
268 **Process effects in the mutant morphospace**
269
270 To assess the extent to which craniofacial shape variation associated with developmental
271 processes aligns with variation from mutants of major effect, we projected 7 process effects onto
272 the first two principal components (PCs) of a dataset containing the DO sample, and samples
273 from 30 mutant genotypes (Fig 5A). Each black label represents the mean shape score of the
274 listed mutant genotype. The shaded ellipse with an orange border displays the 95% confidence
275 ellipse of PCs 1 and 2 of DO cranial shape variation. The DO mean shape is contrasted by the
276 mutant variation along PC1. The first PC describes vault size relative to the length of the face.
277 The phenotype shown along the x-axis of figure 5A depicts the maximum positive PC1 shape,
278 while the heatmap drawn on the crania represents the local deformations towards the minimum

279 PC1 shape. The positive direction of PC2 describes coordinated variation that includes a
280 relatively wider vault, narrower zygomatic, and shorter premaxilla (Fig 5A, y-axis margin).
281
282 Process effects—highlighted with orange vectors originating at the DO mean shape —
283 are necessarily of smaller magnitude than the total variation in the DO sample. Therefore, to
284 better compare the direction of process effects the vector magnitudes were magnified 4x. Several
285 process effects align in distinct directions of mutant effects, such as bmp signaling pathway and
286 endochondral ossification in the direction of *Shh*, *Nipbl*, and *Ift88* mutants. Neurotransmitter
287 transport and Wnt signaling pathway is similar in direction to *Mceph* and *B9d1* mutant effects.
288 Execution phase of apoptosis and intracellular transport both show similar effects to a cluster of
289 Bmp mutants.
290
291 Finally, we show the similarity of 30 process MGP effects to 30 mouse mutant models in
292 figure 5B. The heatmap shows the correlation in direction with yellow/green denoting higher
293 correlation and teal/blue denoting lower correlation. The bottom right of the heatmap
294 (highlighted by a white border) shows a block of mutants for which there are strong process
295 correlations. These are among the most extreme phenotypes along PC1 (Fig 5A) and include
296 mutants for *Nosip, Bmp2, Grm1, Bmp2; Bmp7* transheterozygote*, Bmp7, Ghrhr, Fgf10, and*
297 *Papps2*. The processes most strongly correlated to these mutants are histone methylation,
298 dendrite morphogenesis, chromosome segmentation, vasodilation, and fibroblast growth factor
299 binding.
300
301 There are a set of mutant phenotypes that have generally low correlations to the set of
302 processes chosen. These mutants include *Fgf3, Shh, Nipbl, Disp, Pten, Hhat, and Alk2; Alk3*
303 transheterozygote. Interestingly, this group of mutants vary more along PC2 than PC1 (Fig 5A).
304 Notably, regulation of intracellular protein transport and regulation of cell death are strongly
305 uncorrelated with the majority of mutant directions.
306
307 **Real-time process GP mapping**
308

309 Finally, we provide an online tool to visualize process effects and make comparisons to mutant
310 effects in real time. This application is found at **genopheno.ucalgary.ca/MGP** and can be used
311 for analyses similar to those described in this paper. When the user selects gene ontology terms,
312 the program searches for genotype markers adjacent to each gene listed and uses the selected
313 markers to fit a regularized PLS model. The result is an estimate of the many-to-many
314 relationship between the selected markers and cranial shape variation. The visual outputs include
315 barplots depicting the relative allele effect sizes for each gene in the process and a 3D plot of the
316 corresponding axis of shape variation. Users can compare the effects of different processes and
317 also compare process effects to mutant effects from a provided database of 30 mutant genotypes.
318
319 To illustrate how to use this application, we have provided the graphical user interface
320 used to select the parameters (Fig 6). As an example, in the "Process text" entry field, supply a
321 starting term; we chose "brain." The GO database is then filtered, returning a user-selectable
322 subset of biological process ontology annotation terms in the "Process filter" field. We chose
323 "forebrain morphogenesis," which has 11 associated genes. We chose to magnify the process
324 phenotype vectors 4x and compare the effect to a heterozygous *Ift88* mutant. *Ift88* is a core
325 component of the primary cilia, which are responsible for promoting developmental signals
326 involved in many facets of facial development (Tian et al., 2017). Further, the plots that are
327 generated are interactive. For example, marker loadings can be highlighted and subset by genes
328 of interest (Plotly, 2015). There is further information about using this online tool in the "About
329 this app" tab.
330
331 **Discussion and Conclusion**
332
333 A key goal in genomics is to create tractable genetic explanations for phenotypic variation. In
334 this study, we used a regularized PLS approach to model the joint effects of genomic markers on
335 multivariate craniofacial shape. This innovative approach allows us to address the joint
336 contributions of multiple genes that share ontological characteristic such as pathway membership
337 on craniofacial shape as a multivariate trait. Specifically, we chose markers adjacent to genes
338 annotated under a developmental process of interest. We showed two process MGP analyses in
339 depth, each with distinct phenotypic effects. The chondrocyte differentiation MGP effect mainly

340 showed effects on the shape of the zygomatic and jugal bones with *Ccn3/Nov* as the most highly
341 loaded corresponding marker effect. The FGF signaling MGP effect was less localized in
342 comparison to the chondrocyte differentiation effect. The FGF signaling phenotype was
343 primarily a smaller cranial vault volume with a longer facial outgrowth, broadly similar to the
344 primary axis of shape change during mouse growth and development (Gonzalez et al., 2013).
345 The most highly loaded markers for the FGF signaling effect were related to *Fgf2* and *Flrt2.* We
346 then compared process MGP phenotypic effects to each other, to mutant phenotypes, and the first
347 four principal components of the diversity outbred sample. Each of these comparisons
348 highlighted the integrated structure of phenotypic variation in mouse craniofacial shape. We
349 found that while there are processes with distinct and localized effects, genetic effects generally
350 converge on a limited set of directions in phenotype space. Further, these process effects often
351 correspond with the directions of major mutations known to affect these same processes.
352
353 Many recent studies have addressed the genetics of craniofacial shape in humans and
354 mice (reviewed in: Roosenboom et al., 2016; Weinberg et al., 2018). While these studies are
355 yielding a growing list of genes, suggesting that facial shape is highly polygenic, they have left
356 the vast majority of heritable variation unexplained. Existing studies have either used univariate
357 measures of facial shape such as linear measurements or univariate summaries of multivariate
358 shape (eg. Procrustes distances or PC scores). In addition, most genomic studies of craniofacial
359 shape quantify the effects of each genomic marker independently, with notable exceptions
360 focusing on epistatic effects (e.g. Varón-González et al., 2019). Our approach shares common
361 features with some predecessor GP mapping strategies in which candidate genes/SNPs are
362 selected a priori because of common involvement in a pathway (or other mechanistic cluster)
363 (Claes et al., 2014; Liu et al., 2012; Wang et al., 2010, 2007). In particular, Wang and colleagues
364 selected SNPs based on proximity to genes of interest and effect size to jointly model the
365 pathway-level effects on Parkinson disease data. Their approach is similar to gene-set
366 enrichment analysis, weighing over-representation of statistical effects related to case-control
367 group membership. In contrast, our approach focuses on estimating a multivariate continuous set
368 of craniofacial responses. Importantly, our approach jointly identifies genotype-phenotype axes
369 that maximally covary. This differs significantly from approaches that determine phenotypes for
370 analysis *a priori* or based on a pre-determined method of data reduction such as PCA. Our

371 approach also differs from methods that associate single locus effects with a multivariate
372 phenotype (Claes et al., 2018).
373
374 A key finding of our application of the MGP method to craniofacial shape is that
375 multivariate phenotypic variation aligns nonrandomly to genetic markers associated with
376 pathways or developmental processes. For most process MGP maps, multiple markers for gene
377 sets with known developmental relationships covary in their relationship with craniofacial shapes
378 (Supp fig 2). These covarying effects represent joint genetic effects of multiple contributors to
379 phenotypic variance. While these patterns of multivariate genotype-phenotype covariation may
380 include genetic variants that do not actually affect the phenotype, many others will be
381 contributors that we lack statistical power to detect under a typical univariate approach (Pitchers
382 et al., 2019; Varón-González et al., 2019). Here, the overall pattern of genotype-phenotype
383 covariance is the level of genetic explanation for phenotypic variation. When such patterns
384 involve genes that are ontologically linked in meaningful ways, they provide a level of insight
385 into the developmental-genetics of phenotypic variation that is beyond reach for most genome-
386 wide association studies for complex traits.
387
388 In aggregate, our results show substantial covariance in the directions of phenotypic
389 effects among different developmental processes (Figure 4A). The largest of these captures
390 processes general to development such as cell proliferation or pattern specification. The second
391 captures processes more specific to craniofacial development such as cranial suture/ossification
392 and neural tube patterning. While processes are structured in their effects, our data suggest that
393 many processes likely "add up" to produce variation. Thus, of 1000 randomly selected processes,
394 25.7% had a PC1 correlation higher than 0.6, supporting not only a highly polygenic model of
395 facial variation, but one in which hundreds or even thousands of developmental processes that
396 contribute to craniofacial variation. Importantly, this result shows how many processes and
397 pathways converge to produce central axes of variation in craniofacial shape.
398
399 The explicit modeling of multivariate relationships between phenotypes and genotypes
400 also allows a focus on pleiotropy. Developmental studies in mice demonstrate widespread
401 craniofacial morphological effects from localized developmental perturbations (Martínez-

402 Abadías et al., 2012; Stelzer et al., 2007; Young et al., 2010). Perturbations to specific processes
403 in development generally produce effects on multiple aspects of phenotype due to knock-on
404 effects at later stages or to interactions at the level of tissues or anatomical structures
405 (Hallgrimsson et al, 2007). A change in cartilage growth in basicranial synchondroses produces a
406 global change in craniofacial form, for example (Parsons et al, 2015). Remarkably, enhancers
407 with highly specific temporospatial effects on gene expression also produce global rather than
408 localized changes in craniofacial shape (Attanasio et al., 2013). Given that pleiotropy is likely
409 ubiquitous (Hill and Zhang, 2012; Wagner et al, 2008), explicitly multivariate approaches to
410 understanding genotype-phenotype maps are clearly needed.
411
412 This convergence of genetic effects on axes of covariation is also reflected in our finding
413 that mutations to major developmental genes produce effects that tend to align with the
414 directions of effect associated with the corresponding broader pathways or ontological groups.
415 Our analysis focused on two specific processes— FGF signaling and chondrocyte differentiation.
416 There was a strong correlation between the *Fgf10* mutant and the FGF signaling pathway effect,
417 while the *Alk6* mutant effect was moderately correlated to the chondrocyte differentiation
418 direction. For both process MGP maps, other mouse models in the same pathway showed
419 significant but weaker correlations in direction of effect. These results suggest that perturbations
420 that are developmentally similar tend to move the phenotype in the same direction in multivariate
421 space (Figure 5B). Even so, both mutational and higher-level pathway/process effects tend to
422 converge on a few directions of variation suggesting that multiple pathways and processes lead
423 to common developmental outcomes. This conclusion is further supported by our finding that the
424 genetic axes of covariance for individual processes/pathways can align with multiple directions
425 of mutational effect. For example, the process MGP phenotypes highlighted in the white
426 rectangle in figure 5B are all highly correlated with a set of BMP and growth hormone-related
427 mutants.
428
429 In some cases, mutants and MGP map directions do not correspond. There several
430 reasons why this can occur. The first is that the DO population may simply lack alleles as
431 deleterious as found in mutant lines. A small effect allele in the DO may not align with the
432 direction of a mutant almost completely lacking expression of the target gene. Further, there are

433 many examples where a mutation may have different and sometimes even opposite effects
434 depending on genetic background (Mackay, 2014; Percival et al., 2017). Mutations of major
435 effect may also differ in direction from variants in related genes that have smaller phenotypic
436 effects due to underlying nonlinearities in development (Green et al., 2017). Investigating how
437 variants in genes that are functionally related vary in phenotypic effect is an important avenue of
438 inquiry that is revealed by analyses such as those we have performed here. Additionally,
439 relationships between process and mutant effects may stimulate hypotheses about previously
440 unknown or unvalidated interactions between loci or pathways.
441
442 A second potential reason that MGP effects may not correspond to major mutation effects
443 is the use of only one PLS axis for each process analysis. With only one axis, we select the
444 phenotypic direction with greatest covariance with genetic marker variation. If there are multiple
445 large marker effects that do not covary, the weaker marker effect will be masked in the analysis.
446 For instance, there may be a PLS axis for "FGF signaling" that corresponds more strongly with
447 the *Fgf3* mutant phenotype (Supp fig 3). This phenomenon may be particularly prominent for
448 pathways with substantially different mutant effects, like FGF (Fig 5A).
449
450 Finally, our analysis shares the limitation of all approaches based on gene annotation
451 data. Incomplete annotation may contribute to lead to faulty or incomplete groupings of genes
452 when defining pathway/process hypotheses. Gene annotation is a huge undertaking, and there is
453 substantial variation in the completeness of different process annotations. Many process
454 annotations are manually assigned using inference from the literature, while most are a
455 combination of automated efforts based on transcript similarity and human curation (Mudge and
456 Harrow, 2015). Related to this, we assign gene annotation data to genetic markers based on the
457 closest protein-coding region. While this is a reasonable proxy, there will be regulatory sites that
458 affect genes other than the one immediately adjacent and this is a potential source of uncertainty
459 in our analysis.
460
461 The MGP method represents a deliberate decision to trade higher level insight from
462 genotype-phenotype association data at the expense of statistical certainty about the significance
463 of individual gene effects. The current implementation of the method also does not allow for

464 quantification of individual epistatic effects. Epistasis occurs when the genotypic trait value for a
465 locus is altered by the genotype of a different locus. Such effects generate nonlinear genotype
466 phenotype maps, but when considered genome-wide, contribute mainly to additive variance
467 (Cheverud and Routman, 1995; Hill, 2017). The MGP method is additive in that it models only
468 the linear effects of genes. However, since it captures the covariances among genotypic effects,
469 much of this "additive" variation is likely epistatic in origin.
470
471 Complex traits present a massive challenge in genomics because so many are turning out
472 to be enormously polygenic. To generate tractable explanations of the genetic basis for such
473 traits, methods are needed that extract higher-level representation of genotype-phenotype
474 relationships than those that emerge from single-locus focused approaches. Here, we present a
475 hypothesis-driven framework for deriving such higher-level genetic explanations for phenotypic
476 variation. Our approach leverages the biological tendency for developmental processes to
477 produce covariation among aspects of a multivariate phenotypic trait (Hallgrimsson et al., 2009;
478 Wagner et al., 2007). The underlying assumption in this approach is that there are latent variables
479 within high-dimensional genotype-phenotype data that correspond to developmental architecture.
480 We believe that analyses aimed at defining and characterizing such latent variables represent a
481 level of genetic explanation for phenotypic variation that is complementary to genetic analyses
482 designed to establish the significance of single locus effects. Pursuing such questions will help
483 bridge the gap between emerging mechanistic accounts of morphogenesis and our growing
484 understanding of the genetics of morphological variation.
485
486 **Methods**
487
488 **DO mice**
489
490 We use a sample (n = 1,145) of Diversity Outbred mice (DO; Jackson Laboratory, Bar Harbor,
491 ME) to map GP relationships for craniofacial shape (Churchill et al., 2012, 2004). The DO is a
492 multiparental outcross population derived from the eight founding lines of the Collaborative
493 Cross (CC). Each animal's genome is a unique mosaic of the genetic diversity found in the CC—
494 more than 45 million segregating SNPs (Collaborative Cross Consortium, 2012). Random

outcrossing over many DO generations maintains this diversity and, with recombination, increases mapping resolution.

Our DO sample was sourced from three separate laboratories and seven DO generations. 386 are from the Jackson Laboratory (JAX), 287 from the University of North Carolina (UNC), and 472 come from the Scripps Research Institute. Supplemental figure 4 shows the distribution of the sample by lab source and generation of breeding. Imaging of mice at the University of Calgary was performed under IACUC protocol AC13-0268.

Genotyping

Genotyping was performed by Neogen (Lincoln, NE). Ear clippings were used to extract DNA for all samples. Mice from generations 9, 10, and 15 were genotyped using the MegaMUGA genotyping array (77,808 markers); mice from generations 19, 21, 23, and 27 were genotyped using the larger GigaMUGA array (143,259 markers) (Morgan et al., 2016). To pool the genotype data from these two SNP arrays with differing numbers of markers, we imputed markers between the two genotyping arrays using the "calc_genoprob" function in the qtl2 package (Broman et al., 2018). The function uses a hidden Markov model to estimate genotype probabilities and missing genotype data (Gatti et al., 2014). After imputation, the merged genetic dataset consists of 123,309 SNPs which vary among CC founders. Each animal's genetic record is a 123,309*8 matrix of estimated diplotype contributions of each CC founder to each marker.

Scanning and landmarking

We used micro-computed tomography to acquire 3D scans of the full heads of the mice. Scanning was done at the University of Calgary at .035 mm voxel resolution (Scanco vivaCT40). One of us (WL) then acquired 54 3D landmarks (Fig 7) manually on each volume using Analyze 3D. A discussion of the error associated with manual landmarking can be found in Percival et al (Percival et al., 2019).

Landmark registration

We symmetrized landmarks along the midline of the skull using Klingenberg et al.'s method for object symmetry which configures landmark pairs into a common orientation with reflection and subsequently removes variation associated with translation, scale, and rotation, using Generalized Procrustes Analysis (Adams and Otárola-Castillo, 2013; Klingenberg et al., 2002; Mardia, 2000; Schlager, 2017). To focus on shared, within-generation patterns in our multigenerational DO sample, we regressed symmetric shape on DO generation, and used the residual shapes with the grand mean added as the observations for analysis.

Genetic relatedness

Adjustment of phenotypes for the influence of genetic relatedness is a common approach in genomic studies to prevent spurious associations. However, it is not necessary in all cases, such as situations with low genetic relatedness and little variation in relatedness. We evaluated whether accounting for genetic relatedness was important for our sample. To do so, we estimated a kinship matrix based on DO genotype correlations (Cheng et al., 2013; Broman et al., 2019). The kinship values in our sample have a mean of 0 and a standard deviation of .047 (Supp fig 5). As a result of these findings, we performed all subsequent analyses on the within-generation symmetric shape data, without an adjustment for relatedness.

Regularized PLS analysis

Multivariate genotype-phenotype methods for explicitly modeling multivariate phenotypes and for overcoming the limitations of simple linear regression are increasingly common in mapping studies. Claes et al. (Claes et al., 2018) used canonical correlation analysis to quantify individual SNP effects for a multivariate measurement of facial shape. Each test returns a vector of the linear combination of phenotypic effects that maximally correlates to the alleles at a given locus. Mitteroecker et al. (Mitteroecker et al., 2016) developed a multivariate strategy around a singular value decomposition (SVD) of GP covariation. Partial least squares (PLS) describes a family of approaches that use SVD to decompose cross covariance matrices (Lee et al., 2011; Mitteroecker and Gunz, 2009; Singh et al., 2016). PLS is increasingly used with large genetic datasets in order

557 to model how genomic effects extend to multiple traits (BJØRNSTAD et al., 2004; Mehmood et
558 al., 2011; Tyler et al., 2017). However, its implementation for MGP mapping is, thus far, much
559 more limited.
560
561 SVD decomposes the covariance matrix into three matrices:
562
563 $$\boldsymbol{Y} = \boldsymbol{UDV}'$$
564
565 Where **Y** is the mean-centered covariance matrix, **U** denotes the left singular vectors, a set of
566 vectors of unit length describing the relative weighting of each variable on each axis, and **D**
567 denotes the variance along each axis. **V** denotes the set of right singular vectors. For a full
568 (square, symmetric) covariance matrix, **U** and **V** are identical, and the decomposition is
569 equivalent to PCA. For a non-symmetric matrix of covariances, i.e., one describing covariance
570 between two distinct blocks of traits, each successive column of **U** and **V** provide a pair of
571 singular vectors describing the best least squares approximation of covariance between the two
572 blocks, in order of greatest covariance explained to least.
573
574 PLS is most often used to find low-rank linear combinations that maximize covariance
575 between two sets of features. Here, we use a data-driven regularized PLS model implemented in
576 the mddsPLS package to find paired axes that maximize covariance between allelic and shape
577 variation (Lorenzo et al., 2019). The model uses a lasso penalty to minimize the coefficients
578 (loadings) towards zero to prevent overfitting (James et al., 2013). Overfitting can occur in when
579 many genotypic markers are included in the model, particularly when markers are colinear. The
580 genotype block is composed of the full set of DO founder probabilities for each selected marker.
581 Thus, an analysis of 20 markers would estimate 160 genotype coefficients. The phenotype block
582 consists of the full set of 54 3-dimensional landmarks (162 phenotype coefficients). In all
583 biological process analyses undertaken herein, we used a regularization parameter of 0.06 and
584 report only the first paired axes of the PLS model, i.e., the genotype and phenotype axes which
585 explain the most covariance.
586
587 **Process-specific analysis**

588

589 For process-specific MGP analyses, we used the mouse genome informatics database (Bult et al.,
590 2018) to identify genes annotated to a given process. Each annotation term has an associated GO
591 ID. For example, "chondrocyte differentiation" has GO ID GO:000206 (Fig 2, box 1). We cross-
592 reference the GO ID with the Ensemble genome database (GRCm38.p6) to find the name,
593 chromosome, and base pair start/end position for each gene (Fig 2, box 2) annotated to the
594 process. For genes with multiple splice variants, we select the full transcript start/end positions.
595 For each gene, we compare marker base pair positions and select the closest upstream and
596 downstream markers to the center of each gene. The 8-state genotype probability is then
597 calculated as the average founder allele probabilities between the two selected markers. (Fig 2,
598 box 3). After marker selection, we fit the regularized PLS model using the founder allele
599 probabilities (8 variables/marker) and full landmark data set (Fig 2, box 4).
600

601 We generate graphical displays of process results using the R packages ggplot2
602 (Wickham, 2016) and Morpho (Schlager, 2017). An example script to reproduce the analyses is
603 provided at **github.com/j0vid**.
604

605 **Statistical results and comparisons**
606

607 We estimate the magnitude and direction of MGP process effects using R^2 and vector
608 correlations, respectively. R^2 is calculated as the ratio of trace of the predicted model covariance
609 to the trace of the phenotypic covariance matrix. We contextualize the MGP process R^2 by
610 comparing it to the R^2 value of 1000 randomly drawn marker sets of the same size. For instance,
611 a process annotated with 40 genes would be compared to 1000 40-gene MGP analyses with
612 random markers selected in each iteration. Random marker selection for permutation is
613 constrained to follow similar patterns of linkage disequilibrium to the observed marker set of
614 interest. The null expectation in this scenario is that gene annotation does not provide better
615 information about coordinated marker effects than a randomly selected set of markers.
616

617 Vector correlations between process MGP effects are calculated by taking the Pearson
618 product-moment correlation of the two sets of process PLS1 phenotypic loadings. Vector

correlations between process effects and mutant effects are calculated by taking the correlation between the process PLS1 phenotypic loadings and mutant MANOVA coefficients. The MANOVA compares the mutant group phenotype with the DO sample specified as the reference group.

Visualization tools

We introduce an interactive web application that allows the user to select processes of interest with a graphical user interface and see the resulting craniofacial effect at **genopheno.ucalgary.ca/MGP**. The web apps were written using the shiny package in R (Chang et al., 2018). The application dynamically filters the MGI GO database based on the initial user input. Queries will only list GO terms with exact matches. For example, “chond” will return GO terms that incorporate either “chondrocyte” and “mitochondria”.

Multiple queries can be selected. An analysis of “chondrocyte differentiation” and “chondrocyte hypertrophy” will select the joint gene set of both processes. Processes with different names can be jointly queried with the pipe operator “|”, which is interpreted as an OR (union) operator. For example, to generate the list of GO terms associated with either apoptosis or WNT, we used the “apoptosis|WNT” query and selected the processes “Wnt signaling pathway” and “execution phase of apoptosis” to perform the analysis on the joint set of associated genes (Supp fig 6).

Several other parameters can be specified by the user including the type of plot to be generated for the genetic loadings, the amount of magnification applied to the phenotype effect vectors, the regularization parameter, and the option to overlay a mutant phenotype for comparison. The comparative database currently includes craniofacial shape contrast data (wild-type vs. mutant) for 30 mutant genotypes. If a mutant comparison is selected, the full set of DO specimens are registered with the mutants added (with size removed). We then provide the vector correlation between the process effect and the mutant effect (see Fig 6). The database also includes PC1 of the DO sample for comparison.

The app enables users to save results. A save request will generate and download an HTML report of the analysis which includes several versions of the genetic effect plot and an interactive 3D model of the estimated phenotypic effect. If a mutant comparison is selected, it will also appear in the report.

The application tracks recent searches by the user for their reference. A heatmap of process vector correlations of the PLS phenotype loadings is also available under the "recent searches" tab. The user can select between a heatmap of the processes in their search history or a random assortment of process correlations from past, anonymous user searches.

Acknowledgements:

Grants: NIH - 2R01DE019638 to RM, BH and JC, NSERC 238992-17, CIHR Foundation grant to BH and CFI grant #36262 to BH. JDA is supported by an Eyes High fellowship and an Alberta Children's Hospital Research Institute scholarship.

References

Attanasio C, Nord AS, Zhu Y, Blow MJ, Li Z, Liberton DK, Morrison H, Plajzer-Frick I, Holt A, Hosseini R, Phouanenavong S, Akiyama JA, Shoukry M, Afzal V, Rubin EM, FitzPatrick DR, Ren B, Hallgrímsson B, Pennacchio LA, Visel A. 2013. Fine Tuning of Craniofacial Morphology by Distant-Acting Enhancers. *Science* **342**:1241006. doi:10.1126/science.1241006

Brazil DP, Church RH, Surae S, Godson C, Martin F. 2015. BMP signalling: agony and antagony in the family. *Trends Cell Biol* **25**:249–264. doi:10.1016/j.tcb.2014.12.004

Broman K, Sen Ś. (2009). A Guide to QTL Mapping with R/qtl. Springer. ISBN 978-0-387-92125-9. https://doi.org/10.1007/978-0-387-92125-9

Broman K, Gatti D, Simecek P, Furlotte N, Prins P, Sen Ś, Yandell B, Churchill G. (2018). R/qtl2: Software for Mapping Quantitative Trait Loci with High-Dimensional Data and Multi-parent Populations Genetics 211(2), genetics.301595.2018. https://dx.doi.org/10.1534/genetics.118.301595

Chai Y. 2015. Craniofacial Development. *Current Topics in Dev Bio.* Academic Press. Volume 115. ISBN 9780124081413.

Chebib J, Guillaume F. 2017. What affects the predictability of evolutionary constraints using a G-matrix? The relative effects of modular pleiotropy and mutational correlation. *Evol Int J Org Evol* **71**:2298–2312. doi:10.1111/evo.13320

Cheverud JM, Routman EJ. 1996. EPISTASIS AS A SOURCE OF INCREASED ADDITIVE GENETIC VARIANCE AT POPULATION BOTTLENECKS. *Evolution* **50**:1042–1051. doi:10.1111/j.1558-5646.1996.tb02345.x

Churchill GA, Gatti DM, Munger SC, Svenson KL. 2012. The diversity outbred mouse population. *Mamm Genome* **23**:713–718. doi:10.1007/s00335-012-9414-2

Claes P, Liberton DK, Daniels K, Rosana KM, Quillen EE, Pearson LN, McEvoy B, Bauchet M, Zaidi AA, Yao W, Tang H, Barsh GS, Absher DM, Puts DA, Rocha J, Beleza S, Pereira RW, Baynam G, Suetens P, Vandermeulen D, Wagner JK, Boster JS, Shriver MD. 2014. Modeling 3D Facial Shape from DNA. *Plos Genet* **10**:e1004224. doi:10.1371/journal.pgen.1004224

Claes, P., Roosenboom, J., White, J. D., Swigut, T., Sero, D., Li, J., Lee, M. K., Zaidi, A., Mattern, B. C., Liebowitz, C., Pearson, L., González, T., Leslie, E. J., Carlson, J. C., Orlova, E., Suetens, P., Vandermeulen, D., Feingold, E., Marazita, M. L., Shaffer, J. R., Wysocka, J., Shriver, M. D., & Weinberg, S. M. (2018). Genome-wide mapping of global-to-local genetic effects on human facial shape. *Nature Genetics,* **50**(3), 414-423. doi:10.1038/s41588-018-0057-4

Cole, J. B., Manyama, M., Kimwaga, E., Mathayo, J., Larson, J. R., Liberton, D. K., Lukowiak, K., Ferrara, T. M., Riccardi, S. L., Li, M., Mio, W., Prochazkova, M., Williams, T., Li, H., Jones, K. L., Klein, O. D., Santorico, S. A., Hallgrimsson, B., & Spritz, R. A. (2016). Genomewide Association Study of African Children Identifies Association of SCHIP1 and PDE8A with Facial Size and Shape. *PLoS Genetics*, **12**(8), e1006174. doi:10.1371/journal.pgen.1006174

Cole JB, Manyama M, Larson JR, Liberton DK, Ferrara TM, Riccardi SL, Li M, Mio W, Klein OD, Santorico SA, Hallgrímsson B, Spritz RA. 2017. Human Facial Shape and Size Heritability and Genetic Correlations. *Genetics* **205**:967–978. doi:10.1534/genetics.116.193185

Collaborative Cross Consortium. 2012. The Genome Architecture of the Collaborative Cross Mouse Genetic Reference Population. *Genetics* **190**:389–401. doi:10.1534/genetics.111.132639

Dudbridge F. 2013. Power and Predictive Accuracy of Polygenic Risk Scores. *Plos Genet* **9**:e1003348. doi:10.1371/journal.pgen.1003348

FANTOM Consortium, Forrest ARR, Kawaji H, Rehli M, Baillie JK, Hoon MJL de, Haberle V, Lassmann T, Kulakovskiy IV, Lizio M, Itoh M, Andersson R, Mungall CJ, Meehan TF, Schmeier S, Bertin N, Jørgensen M, Dimont E, Arner E, Schmidl C, Schaefer U, Medvedeva YA, Plessy C, Vitezic M, Severin J, Semple CA, Ishizu Y, Young RS, Francescatto M, Alam I, Albanese D, Altschuler GM, Arakawa T, Archer JAC, Arner P, Babina M, Rennie S, Balwierz PJ, Beckhouse AG, Pradhan-Bhatt S, Blake JA, Blumenthal A, Bodega B, Bonetti A, Briggs J, Brombacher F, Burroughs AM, Califano A, Cannistraci CV, Carbajo D, Chen Y, Chierici M, Ciani Y, Clevers HC, Dalla E, Davis CA, Detmar M, Diehl AD, Dohi T, Drabløs F, Edge ASB, Edinger M, Ekwall K, Endoh M, Enomoto H, Fagiolini M, Fairbairn L, Fang H, Farach-Carson MC, Faulkner GJ, Favorov AV, Fisher ME, Frith MC, Fujita R, Fukuda S, Furlanello C, Furuno M, Furusawa J, Geijtenbeek TB, Gibson AP, Gingeras T, Goldowitz D, Gough J, Guhl S, Guler R, Gustincich S, Ha TJ, Hamaguchi M, Hara M, Harbers M, Harshbarger J, Hasegawa A, Hasegawa Y, Hashimoto T, Herlyn M, Hitchens KJ, Sui SJH, Hofmann OM, Hoof I, Hori F, Huminiecki L, Iida K, Ikawa T, Jankovic BR, Jia H, Joshi A, Jurman G, Kaczkowski B, Kai C, Kaida K, Kaiho A, Kajiyama K, Kanamori-Katayama M, Kasianov AS, Kasukawa T, Katayama S, Kato S, Kawaguchi S, Kawamoto H, Kawamura YI, Kawashima T, Kempfle JS, Kenna TJ, Kere J, Khachigian LM, Kitamura T, Klinken SP, Knox AJ, Kojima M, Kojima S, Kondo N, Koseki H, Koyasu S, Krampitz S, Kubosaki A, Kwon AT, Laros JFJ, Lee W, Lennartsson A, Li K, Lilje B, Lipovich L, Mackay-sim A, Manabe R, Mar JC, Marchand B, Mathelier A, Mejhert N, Meynert A, Mizuno Y, Morais DA de L, Morikawa H, Morimoto M, Moro K, Motakis E, Motohashi H, Mummery CL, Murata M, Nagao-Sato S, Nakachi Y, Nakahara F, Nakamura T, Nakamura Y, Nakazato K, Nimwegen E van, Ninomiya N, Nishiyori H, Noma S, Nozaki T, Ogishima S, Ohkura N, Ohmiya H, Ohno H, Ohshima M, Okada-Hatakeyama M, Okazaki Y, Orlando V, Ovchinnikov DA, Pain A, Passier R, Patrikakis M, Persson H, Piazza S, Prendergast JGD, Rackham OJL, Ramilowski JA, Rashid M, Ravasi T, Rizzu P, Roncador M, Roy S, Rye MB, Saijyo E, Sajantila A, Saka A, Sakaguchi S, Sakai M, Sato H, Satoh H, Savvi S, Saxena A,

744 Schneider C, Schultes EA, Schulze-Tanzil GG, Schwegmann A, Sengstag T, Sheng G,
745 Shimoji H, Shimoni Y, Shin JW, Simon C, Sugiyama D, Sugiyama T, Suzuki M, Suzuki N,
746 Swoboda RK, Hoen PAC 't, Tagami M, Takahashi N, Takai J, Tanaka H, Tatsukawa H,
747 Tatum Z, Thompson M, Toyoda H, Toyoda T, Valen E, Wetering M van de, Berg LM van
748 den, Verardo R, Vijayan D, Vorontsov IE, Wasserman WW, Watanabe S, Wells CA,
749 Winteringham LN, Wolvetang E, Wood EJ, Yamaguchi Y, Yamamoto M, Yoneda M,
750 Yonekura Y, Yoshida S, Zabierowski SE, Zhang PG, Zhao X, Zucchelli S, Summers KM,
751 Suzuki H, Daub CO, Kawai J, Heutink P, Hide W, Freeman TC, Lenhard B, Bajic VB, Taylor
752 MS, Makeev VJ, Sandelin A, Hume DA, Carninci P, Hayashizaki Y. 2014. A promoter-level
753 mammalian expression atlas. *Nature* **507**:462. doi:10.1038/nature13182

754 Finger JH, Smith CM, Hayamizu TF, McCright IJ, Xu J, Law M, Shaw DR, Baldarelli RM, Beal
755 JS, Blodgett O, Campbell JW, Corbani LE, Lewis JR, Forthofer KL, Frost PJ, Giannatto SC,
756 Hutchins LN, Miers DB, Motenko H, Stone KR, Eppig JT, Kadin JA, Richardson JE,
757 Ringwald M. 2017. The mouse Gene Expression Database (GXD): 2017 update. *Nucleic*
758 *Acids Res* **45**:D730–D736. doi:10.1093/nar/gkw1073

759 Francis-West P, Crespo-Enriquez I. 2016. Vertebrate Embryo: Craniofacial Development. *eLS*
760 1–15. doi:10.1002/9780470015902.a0026602

761 Gasch AP, Payseur BA, Pool JE. 2016. The Power of Natural Variation for Model Organism
762 Biology. *Trends Genet* **32**:147–154. doi:10.1016/j.tig.2015.12.003

763 Gatti DM, Svenson KL, Shabalin A, Wu L-Y, Valdar W, Simecek P, Goodwin N, Cheng R,
764 Pomp D, Palmer A, Chesler EJ, Broman KW, Churchill GA. 2014. Quantitative Trait Locus
765 Mapping Methods for Diversity Outbred Mice. *G3 Genes Genomes Genetics* **4**:1623–1633.
766 doi:10.1534/g3.114.013748

767 Gonzalez, PN, Kristensen, E, Morck, DW, Boyd, S, Hallgrímsson, B. 2013. Effects of growth
768 hormone on the ontogenetic allometry of craniofacial bones. *Evolution & Development* **15**:
769 133-145. doi:10.1111/ede.12025

770 Green RM, Fish JL, Young NM, Smith FJ, Roberts B, Dolan K, Choi I, Leach CL, Gordon P,
771 Cheverud JM, Roseman CC, Williams TJ, Marcucio RS, Hallgrímsson B. 2017.
772 Developmental nonlinearity drives phenotypic robustness. *Nat Commun* **8**:1970.
773 doi:10.1038/s41467-017-02037-7

774 Hallgrimsson, B, Lieberman, DE, Liu, W, Ford-Hutchinson, AF, Jirik, FR. 2007. Epigenetic
775 interactions and the structure of phenotypic variation in the cranium. *Evol Dev* **9**(1), 76-91.

776 Hallgrimsson B, Green RM, Katz DC, Fish JL, Bernier FP, Roseman CC, Young NM, Cheverud
777 JM, Marcucio RS. 2018. The developmental-genetics of canalization. *Semin Cell Dev Biol*.
778 doi:10.1016/j.semcdb.2018.05.019

779 Hallgrímsson B, Jamniczky H, Young NM, Rolian C, Parsons TE, Boughner JC, Marcucio RS.
780 2009. Deciphering the Palimpsest: Studying the Relationship Between Morphological

781 Integration and Phenotypic Covariation. *Evol Biol* **36**:355–376. doi:10.1007/s11692-009-
782 9076-5

783 Hallgrímsson B, Lieberman DE. 2008. Mouse models and the evolutionary developmental
784 biology of the skull. *Integr Comp Biol* **48**:373–384. doi:10.1093/icb/icn076

785 Hallgrimsson B, Mio W, Marcucio RS, Spritz R. 2014. Let's Face It—Complex Traits Are Just
786 Not That Simple. *Plos Genet* **10**:e1004724. doi:10.1371/journal.pgen.1004724

787 Hilliard SA, Yu L, Gu S, Zhang Z, Chen YP. 2005. Regional regulation of palatal growth and
788 patterning along the anterior–posterior axis in mice. *J Anat* **207**:655–667. doi:10.1111/j.1469-
789 7580.2005.00474.x

790 Houle D, Fierst J. 2012. Properties of spontaneous mutational variance and covariance for wing
791 size and shape in Drosophila melanogaster. *Evol Int J Org Evol* **67**:1116–30.
792 doi:10.1111/j.1558-5646.2012.01838.x

793 Houle D, Govindaraju DR, Omholt S. 2010. Phenomics: the next challenge. *Nat Rev Genet*
794 **11**:855. doi:10.1038/nrg2897

795 Jin Y-R, Han XH, Taketo MM, Yoon JK. 2012. Wnt9b-dependent FGF signaling is crucial for
796 outgrowth of the nasal and maxillary processes during upper jaw and lip development.
797 *Development* **139**:1821–1830. doi:10.1242/dev.075796

798 Johannsdottir B, Thorarinsson F, Thordarson A, Magnusson TE. 2005. Heritability of
799 craniofacial characteristics between parents and offspring estimated from lateral
800 cephalograms. *Am J Orthod Dentofac* **127**:200–207. doi:10.1016/j.ajodo.2004.07.033

801 Kanehisa M, Furumichi M, Tanabe M, Sato Y, Morishima K. 2017. KEGG: new perspectives on
802 genomes, pathways, diseases and drugs. *Nucleic Acids Res* **45**:D353–D361.
803 doi:10.1093/nar/gkw1092

804 Katz DC, Aponte JD, Liu W, Green RM, Mayeux JM, Pollard KM, Pomp D, Munger SC,
805 Murray SA, Roseman CC, Percival CJ, Cheverud J, Marcucio RS, Hallgrímsson B. 2019.
806 Facial shape and allometry quantitative trait locus intervals in the Diversity Outbred mouse
807 are enriched for known skeletal and facial development genes. *Biorxiv* 787291.
808 doi:10.1101/787291

809 Kawauchi S, Calof AL, Santos R, Lopez-Burks ME, Young CM, Hoang MP, Chua A, Lao T,
810 Lechner MS, Daniel JA, Nussenzweig A, Kitzes L, Yokomori K, Hallgrimsson B, Lander
811 AD. 2009. Multiple Organ System Defects and Transcriptional Dysregulation in the Nipbl+/−
812 Mouse, a Model of Cornelia de Lange Syndrome. *Plos Genet* **5**:e1000650.
813 doi:10.1371/journal.pgen.1000650

814 Kenney-Hunt JP, Wang B, Norgard EA, Fawcett G, Falk D, Pletscher LS, Jarvis JP, Roseman C,
815 Wolf J, Cheverud JM. 2008. Pleiotropic Patterns of Quantitative Trait Loci for 70 Murine
816 Skeletal Traits. *Genetics* **178**:2275–2288. doi:10.1534/genetics.107.084434

817 Klingenberg CP, Leamy LJ. 2001. QUANTITATIVE GENETICS OF GEOMETRIC SHAPE IN
818 THE MOUSE MANDIBLE. *Evolution* **55**:2342–2352. doi:10.1554/0014-
819 3820(2001)055[2342:qgogsi]2.0.co;2

820 Lewontin R. 1974. The Genetic Basis of Evolutionary Change. New York, Columbia University
821 Press, 1974.

822 Liu F, Lijn F van der, Schurmann C, Zhu G, Chakravarty MM, Hysi PG, Wollstein A, Lao O,
823 Bruijne M de, Ikram MA, Lugt A van der, Rivadeneira F, Uitterlinden AG, Hofman A,
824 Niessen WJ, Homuth G, Zubicaray G de, McMahon KL, Thompson PM, Daboul A, Puls R,
825 Hegenscheid K, Bevan L, Pausova Z, Medland SE, Montgomery GW, Wright MJ, Wicking
826 C, Boehringer S, Spector TD, Paus T, Martin NG, Biffar R, Kayser M. 2012. A Genome-
827 Wide Association Study Identifies Five Loci Influencing Facial Morphology in Europeans.
828 *Plos Genet* **8**:e1002932. doi:10.1371/journal.pgen.1002932

829 Liu W, Sun X, Braut A, Mishina Y, Behringer RR, Mina M, Martin JF. 2005. Distinct functions
830 for Bmp signaling in lip and palate fusion in mice. *Development* **132**:1453–1461.
831 doi:10.1242/dev.01676

832 Lorenzo H, Saracco J, Thiébaut R. 2019. Supervised Learning for Multi-Block Incomplete Data.
833 arXiv preprint *arXiv*:1901.04380. http://arxiv.org/abs/1901.04380

834 Mackay, T. Epistasis and quantitative traits: using model organisms to study gene–gene
835 interactions.*Nat Rev Genet* **15,** 22–33 (2014). https://doi.org/10.1038/nrg3627

836 Mackay TF, Moore JH. 2014. Why epistasis is important for tackling complex human disease
837 genetics. *Genome Med* **6**:42. doi:10.1186/gm561

838 Maga AM, Navarro N, Cunningham ML, Cox TC. 2015. Quantitative trait loci affecting the 3D
839 skull shape and size in mouse and prioritization of candidate genes in-silico. *Front Physiol*
840 **6**:92. doi:10.3389/fphys.2015.00092

841 Martínez-Abadías N, Mitteroecker P, Parsons TE, Esparza M, Sjøvold T, Rolian C, Richtsmeier
842 JT, Hallgrímsson B. 2012. The Developmental Basis of Quantitative Craniofacial Variation in
843 Humans and Mice. *Evol Biol* **39**:554–567. doi:10.1007/s11692-012-9210-7

844 Mattick JS, Taft RJ, Faulkner GJ. 2010. A global view of genomic information – moving beyond
845 the gene and the master regulator. *Trends Genet* **26**:21–28. doi:10.1016/j.tig.2009.11.002

846 Mitteroecker P, Cheverud JM, Pavlicev M. 2016. Multivariate Analysis of Genotype–Phenotype
847 Association. *Genetics* **202**:1345–1363. doi:10.1534/genetics.115.181339

848 Morozova TV, Huang W, Pray VA, Whitham T, Anholt RRH, Mackay TFC. 2015.
849 Polymorphisms in early neurodevelopmental genes affect natural variation in alcohol
850 sensitivity in adult drosophila. *Bmc Genomics* **16**:865. doi:10.1186/s12864-015-2064-5

851 Mudge JM, Harrow J. 2015. Creating reference gene annotation for the mouse C57BL6/J
852 genome assembly. *Mamm Genome* **26**:366–378. doi:10.1007/s00335-015-9583-x

853 Nakata M. 1985. Twin Studies in Craniofacial Genetics: A Review. *Amg Acta Geneticae*
854 *Medicae Et Gemellologiae Twin Res* **34**:1–14. doi:10.1017/s0001566000004876

855 Ornitz DM, Marie PJ. 2015. Fibroblast growth factor signaling in skeletal development and
856 disease. *Gene Dev* **29**:1463–1486. doi:10.1101/gad.266551.115

857 Pallares LF, Carbonetto P, Gopalakrishnan S, Parker CC, Ackert-Bicknell CL, Palmer AA, Tautz
858 D. 2015. Mapping of Craniofacial Traits in Outbred Mice Identifies Major Developmental
859 Genes Involved in Shape Determination. *Plos Genet* **11**:e1005607.
860 doi:10.1371/journal.pgen.1005607

861 Pallares LF, Harr B, Turner LM, Tautz D. 2014. Use of a natural hybrid zone for genomewide
862 association mapping of craniofacial traits in the house mouse. *Mol Ecol* **23**:5756–5770.
863 doi:10.1111/mec.12968

864 Parsons, T. E., Downey, C. M., Jirik, F. R., Hallgrimsson, B., & Jamniczky, H. A. (2015). Mind
865 the Gap: Genetic Manipulation of Basicranial Growth within Synchondroses Modulates
866 Calvarial and Facial Shape in Mice through Epigenetic Interactions. *PloS One, 10*(2),
867 e0118355. doi:10.1371/journal.pone.0118355

868 Percival CJ, Marangoni P, Tapaltsyan V, Klein O, Hallgrímsson B. 2017. The Interaction of
869 Genetic Background and Mutational Effects in Regulation of Mouse Craniofacial Shape. *G3*
870 *Genes Genomes Genetics* **7**:1439–1450. doi:10.1534/g3.117.040659

871 Percival CJ, Richtsmeier JT. 2013. Angiogenesis and intramembranous osteogenesis. *Dev*
872 *Dynam* **242**:909–922. doi:10.1002/dvdy.23992

873 Pitchers W, Nye J, Márquez EJ, Kowalski A, Dworkin I, Houle D. 2019. A Multivariate
874 Genome-Wide Association Study of Wing Shape in Drosophila melanogaster. *Genetics*
875 **211**:genetics.301342.2018. doi:10.1534/genetics.118.301342

876 Plotly Technologies Inc. Collaborative data science. Montréal, QC, 2015. https://plot.ly.

877 Prochazkova M, Prochazka J, Marangoni P, Klein OD. 2018. Bones, Glands, Ears and More:
878 The Multiple Roles of FGF10 in Craniofacial Development. *Frontiers Genetics* **9**:542.
879 doi:10.3389/fgene.2018.00542

880 R Core Team (2017). R: A language and environment for statistical computing. R Foundation for
881 Statistical Computing, Vienna, Austria. URL https://www.R-project.org/.

882 Reed LK, Baer CF, Edison AS. 2017. Considerations when choosing a genetic model organism
883 for metabolomics studies. *Curr Opin Chem Biol* **36**:7–14. doi:10.1016/j.cbpa.2016.12.005

884 Rendel, J. M. (1967). *Canalization and gene control*. London: Logos Press.

885 Richman JM, Herbert M, Matovinovic E, Walin J. 1997. Effect of Fibroblast Growth Factors on
886 Outgrowth of Facial Mesenchyme. *Dev Biol* **189**:135–147. doi:10.1006/dbio.1997.8656

887 Richtsmeier JT, Flaherty K. 2013. Hand in glove: brain and skull in development and
888 dysmorphogenesis. *Acta Neuropathol* **125**:469–489. doi:10.1007/s00401-013-1104-y

889 Rie D de, Abugessaisa I, Alam T, Arner E, Arner P, Ashoor H, Åström G, Babina M, Bertin N,
890 Burroughs AM, Carlisle AJ, Daub CO, Detmar M, Deviatiiarov R, Fort A, Gebhard C,
891 Goldowitz D, Guhl S, Ha TJ, Harshbarger J, Hasegawa A, Hashimoto K, Herlyn M, Heutink
892 P, Hitchens KJ, Hon CC, Huang E, Ishizu Y, Kai C, Kasukawa T, Klinken P, Lassmann T,
893 Lecellier C-H, Lee W, Lizio M, Makeev V, Mathelier A, Medvedeva YA, Mejhert N,
894 Mungall CJ, Noma S, Ohshima M, Okada-Hatakeyama M, Persson H, Rizzu P, Roudnicky F,
895 Sætrom P, Sato H, Severin J, Shin JW, Swoboda RK, Tarui H, Toyoda H, Vitting-Seerup K,
896 Winteringham L, Yamaguchi Y, Yasuzawa K, Yoneda M, Yumoto N, Zabierowski S, Zhang
897 PG, Wells CA, Summers KM, Kawaji H, Sandelin A, Rehli M, Consortium TF, Hayashizaki
898 Y, Carninci P, Forrest ARR, Hoon MJL de. 2017. An integrated expression atlas of miRNAs
899 and their promoters in human and mouse. *Nat Biotechnol* **35**:nbt.3947. doi:10.1038/nbt.3947

900 Roosenboom J, Hens G, Mattern BC, Shriver MD, Claes P. 2016. Exploring the Underlying
901 Genetics of Craniofacial Morphology through Various Sources of Knowledge. *Biomed Res*
902 *Int* **2016**:1–9. doi:10.1155/2016/3054578

903 Shaffer, J. R., Orlova, E., Lee, M. K., Leslie, E. J., Raffensperger, Z. D., Heike, C. L.,
904 Cunningham, M. L., Hecht, J. T., Kau, C. H., Nidey, N. L., Moreno, L. M., Wehby, G. L.,
905 Murray, J. C., Laurie, C. A., Laurie, C. C., Cole, J., Ferrara, T., Santorico, S., Klein, O., Mio,
906 W., Feingold, E., Hallgrimsson, B., Spritz, R. A., Marazita, M. L., & Weinberg, S. M. (2016).
907 Genome-Wide Association Study Reveals Multiple Loci Influencing Normal Human Facial
908 Morphology. *PLoS Genetics*, **12**(8), e1006149. doi:10.1371/journal.pgen.1006149

909 Schoenfelder S, Javierre B-M, Furlan-Magaril M, Wingett SW, Fraser P. 2018. Promoter
910 Capture Hi-C: High-resolution, Genome-wide Profiling of Promoter Interactions. *J Vis Exp*
911 *Jove* 57320. doi:10.3791/57320

912 Sprinzak E, Margalit H. 2001. Correlated sequence-signatures as markers of protein-protein
913 interaction1 1Edited by G. von Heijne. *J Mol Biol* **311**:681–692. doi:10.1006/jmbi.2001.4920

914 Stelzer C, Brimmer A, Hermanns P, Zabel B, Dietz UH. 2007. Expression profile of Papss2 (3′-
915 phosphoadenosine 5′-phosphosulfate synthase 2) during cartilage formation and skeletal
916 development in the mouse embryo. *Dev Dynam* **236**:1313–1318. doi:10.1002/dvdy.21137

917 Tian H, Feng J, Li J, Ho T-V, Yuan Y, Liu Y, Brindopke F, Figueiredo JC, Magee W, Sanchez-
918 Lara PA, Chai Y. 2017. Intraflagellar transport 88 (IFT88) is crucial for craniofacial
919 development in mice and is a candidate gene for human cleft lip and palate. *Hum Mol Genet*
920 ddx002. doi:10.1093/hmg/ddx002

921 Tsagkrasoulis D, Hysi P, Spector T, Montana G. 2017. Heritability maps of human face
922 morphology through large-scale automated three-dimensional phenotyping. *Sci Rep-uk*
923 **7**:45885. doi:10.1038/srep45885

924 Uller T, Moczek AP, Watson RA, Brakefield PM, Laland KN. 2018. Developmental Bias and
925 Evolution: A Regulatory Network Perspective. *Genetics* **209**:949–966.
926 doi:10.1534/genetics.118.300995

927 Varón-González C, Pallares LF, Debat V, Navarro N. 2019. Mouse Skull Mean Shape and Shape
928 Robustness Rely on Different Genetic Architectures and Different Loci. *Frontiers Genetics*
929 **10**:64. doi:10.3389/fgene.2019.00064

930 Vidal M, Cusick ME, Barabási A-L. 2011. Interactome Networks and Human Disease. *Cell*
931 **144**:986–998. doi:10.1016/j.cell.2011.02.016

932 Visscher PM. 2008. Sizing up human height variation. *Nat Genet* **40**:ng0508-489.
933 doi:10.1038/ng0508-489

934 Visscher PM, Wray NR, Zhang Q, Sklar P, McCarthy MI, Brown MA, Yang J. (2017). 10 Years
935 of GWAS Discovery: Biology, Function, and Translation. *Am J Hum Genetics.* **101**:1:5-22.
936 https://doi.org/10.1016/j.ajhg.2017.06.005

937 Wagner, G., Pavlicev, M., Cheverud, J. (2007). The road to modularity. *Nat Rev Genet* **8**(12),
938 nrg2267. https://dx.doi.org/10.1038/nrg2267

939 Wagner GP, Zhang J. 2011. The pleiotropic structure of the genotype–phenotype map: the
940 evolvability of complex organisms. *Nat Rev Genet* **12**:204. doi:10.1038/nrg2949

941 Wang K, Li M, Bucan M. 2007. Pathway-Based Approaches for Analysis of Genomewide
942 Association Studies. *Am J Hum Genetics* **81**:1278–1283. doi:10.1086/522374

943 Wang K, Li M, Hakonarson H. 2010. Analysing biological pathways in genome-wide association
944 studies. *Nat Rev Genet* **11**:843. doi:10.1038/nrg2884

945 Watson J, Francavilla C. 2018. Regulation of FGF10 Signaling in Development and Disease.
946 *Frontiers Genetics* **9**:500. doi:10.3389/fgene.2018.00500

947 Weinberg SM, Cornell R, Leslie EJ. 2018. Craniofacial genetics: Where have we been and where
948 are we going? *Plos Genet* **14**:e1007438. doi:10.1371/journal.pgen.1007438

Wood AR, Esko T, Yang J, Vedantam S, Pers TH, Gustafsson S, Chu AY, Estrada K, Luan J, Kutalik Z, Amin N, Buchkovich ML, Croteau-Chonka DC, Day FR, Duan Y, Fall T, Fehrmann R, Ferreira T, Jackson AU, Karjalainen J, Lo KS, Locke AE, Mägi R, Mihailov E, Porcu E, Randall JC, Scherag A, Vinkhuyzen AAE, Westra H-J, Winkler TW, Workalemahu T, Zhao JH, Absher D, Albrecht E, Anderson D, Baron J, Beekman M, Demirkan A, Ehret GB, Feenstra B, Feitosa MF, Fischer K, Fraser RM, Goel A, Gong J, Justice AE, Kanoni S, Kleber ME, Kristiansson K, Lim U, Lotay V, Lui JC, Mangino M, Leach IM, Medina-Gomez C, Nalls MA, Nyholt DR, Palmer CD, Pasko D, Pechlivanis S, Prokopenko I, Ried JS, Ripke S, Shungin D, Stancáková A, Strawbridge RJ, Sung YJ, Tanaka T, Teumer A, Trompet S, Laan SW van der, Setten J van, Vliet-Ostaptchouk JVV, Wang Z, Yengo L, Zhang W, Afzal U, Ärnlöv J, Arscott GM, Bandinelli S, Barrett A, Bellis C, Bennett AJ, Berne C, Blüher M, Bolton JL, Böttcher Y, Boyd HA, Bruinenberg M, Buckley BM, Buyske S, Caspersen IH, Chines PS, Clarke R, Claudi-Boehm S, Cooper M, Daw EW, Jong PAD, Deelen J, Delgado G, Denny JC, Dhonukshe-Rutten R, Dimitriou M, Doney ASF, Dörr M, Eklund N, Eury E, Folkersen L, Garcia ME, Geller F, Giedraitis V, Go AS, Grallert H, Grammer TB, Gräßler J, Grönberg H, Groot LCPGM de, Groves CJ, Haessler J, Hall P, Haller T, Hallmans G, Hannemann A, Hartman CA, Hassinen M, Hayward C, Heard-Costa NL, Helmer Q, Hemani G, Henders AK, Hillege HL, Hlatky MA, Hoffmann W, Hoffmann P, Holmen O, Houwing-Duistermaat JJ, Illig T, Isaacs A, James AL, Jeff J, Johansen B, Johansson Å, Jolley J, Juliusdottir T, Junttila J, Kho AN, Kinnunen L, Klopp N, Kocher T, Kratzer W, Lichtner P, Lind L, Lindström J, Lobbens S, Lorentzon M, Lu Y, Lyssenko V, Magnusson PKE, Mahajan A, Maillard M, McArdle WL, McKenzie CA, McLachlan S, McLaren PJ, Menni C, Merger S, Milani L, Moayyeri A, Monda KL, Morken MA, Müller G, Müller-Nurasyid M, Musk AW, Narisu N, Nauck M, Nolte IM, Nöthen MM, Oozageer L, Pilz S, Rayner NW, Renstrom F, Robertson NR, Rose LM, Roussel R, Sanna S, Scharnagl H, Scholtens S, Schumacher FR, Schunkert H, Scott RA, Sehmi J, Seufferlein T, Shi J, Silventoinen K, Smit JH, Smith AV, Smolonska J, Stanton AV, Stirrups K, Stott DJ, Stringham HM, Sundström J, Swertz MA, Syvänen A-C, Tayo BO, Thorleifsson G, Tyrer JP, Dijk S van, Schoor NM van, Velde N van der, Heemst D van, Oort FVA van, Vermeulen SH, Verweij N, Vonk JM, Waite LL, Waldenberger M, Wennauer R, Wilkens LR, Willenborg C, Wilsgaard T, Wojczynski MK, Wong A, Wright AF, Zhang Q, Arveiler D, Bakker SJL, Beilby J, Bergman RN, Bergmann S, Biffar R, Blangero J, Boomsma DI, Bornstein SR, Bovet P, Brambilla P, Brown MJ, Campbell H, Caulfield MJ, Chakravarti A, Collins R, Collins FS, Crawford DC, Cupples LA, Danesh J, Faire U de, Ruijter HM den, Erbel R, Erdmann J, Eriksson JG, Farrall M, Ferrannini E, Ferrières J, Ford I, Forouhi NG, Forrester T, Gansevoort RT, Gejman PV, Gieger C, Golay A, Gottesman O, Gudnason V, Gyllensten U, Haas DW, Hall AS, Harris TB, Hattersley AT, Heath AC, Hengstenberg C, Hicks AA, Hindorff LA, Hingorani AD, Hofman A, Hovingh GK, Humphries SE, Hunt SC, Hypponen E, Jacobs KB, Jarvelin M-R, Jousilahti P, Jula AM, Kaprio J, Kastelein JJP, Kayser M, Kee F, Keinanen-Kiukaanniemi SM, Kiemeney LA, Kooner JS, Kooperberg C, Koskinen S, Kovacs P, Kraja AT, Kumari M, Kuusisto J, Lakka TA, Langenberg C, Marchand LL, Lehtimäki T, Lupoli S, Madden PAF, Männistö S, Manunta P, Marette A, Matise TC, McKnight B, Meitinger T, Moll FL, Montgomery GW, Morris AD, Morris AP, Murray JC, Nelis M, Ohlsson C, Oldehinkel AJ, Ong KK, Ouwehand WH, Pasterkamp G, Peters A, Pramstaller PP, Price JF, Qi L, Raitakari OT, Rankinen T, Rao DC, Rice TK, Ritchie M, Rudan I, Salomaa V, Samani NJ, Saramies J, Sarzynski MA, Schwarz PEH, Sebert S, Sever P, Shuldiner AR, Sinisalo J, Steinthorsdottir V,

995 Stolk RP, Tardif J-C, Tönjes A, Tremblay A, Tremoli E, Virtamo J, Vohl M-C, Consortium
996 TEMR and G (eMERGE), Consortium TMig, Consortium TP, Study TLC, Amouyel P,
997 Asselbergs FW, Assimes TL, Bochud M, Boehm BO, Boerwinkle E, Bottinger EP, Bouchard
998 C, Cauchi S, Chambers JC, Chanock SJ, Cooper RS, Bakker PIW de, Dedoussis G, Ferrucci
999 L, Franks PW, Froguel P, Groop LC, Haiman CA, Hamsten A, Hayes MG, Hui J, Hunter DJ,
1000 Hveem K, Jukema JW, Kaplan RC, Kivimaki M, Kuh D, Laakso M, Liu Y, Martin NG, März
1001 W, Melbye M, Moebus S, Munroe PB, Njølstad I, Oostra BA, Palmer CNA, Pedersen NL,
1002 Perola M, Pérusse L, Peters U, Powell JE, Power C, Quertermous T, Rauramaa R, Reinmaa E,
1003 Ridker PM, Rivadeneira F, Rotter JI, Saaristo TE, Saleheen D, Schlessinger D, Slagboom PE,
1004 Snieder H, Spector TD, Strauch K, Stumvoll M, Tuomilehto J, Uusitupa M, Harst P van der,
1005 Völzke H, Walker M, Wareham NJ, Watkins H, Wichmann H-E, Wilson JF, Zanen P,
1006 Deloukas P, Heid IM, Lindgren CM, Mohlke KL, Speliotes EK, Thorsteinsdottir U, Barroso
1007 I, Fox CS, North KE, Strachan DP, Beckmann JS, Berndt SI, Boehnke M, Borecki IB,
1008 McCarthy MI, Metspalu A, Stefansson K, Uitterlinden AG, Duijn CM van, Franke L, Willer
1009 CJ, Price AL, Lettre G, Loos RJF, Weedon MN, Ingelsson E, O'Connell JR, Abecasis GR,
1010 Chasman DI, Goddard ME, Visscher PM, Hirschhorn JN, Frayling TM. 2014. Defining the
1011 role of common variation in the genomic and biological architecture of adult human height.
1012 *Nat Genet* **46**:ng.3097. doi:10.1038/ng.3097

1013 Wray NR, Goddard ME, Visscher PM. 2007. Prediction of individual genetic risk to disease
1014 from genome-wide association studies. *Genome Res* **17**:1520–1528. doi:10.1101/gr.6665407

1015 Wray NR, Yang J, Hayes BJ, Price AL, Goddard ME, Visscher PM. 2013. Pitfalls of predicting
1016 complex traits from SNPs. *Nat Rev Genet* **14**:nrg3457. doi:10.1038/nrg3457

1017 Yang, J., Benyamin, B., McEvoy, B. P., Gordon, S., Henders, A. K., Nyholt, D. R., Madden, P.
1018 A., Heath, A. C., Martin, N. G., Montgomery, G. W., Goddard, M. E., & Visscher, P. M.
1019 (2010). Common SNPs explain a large proportion of the heritability for human height. *Nat*
1020 *Genet,* **42**(7), 565-569. doi:ng.608

1021 Andrew D Yates, Premanand Achuthan, Wasiu Akanni, James Allen, Jamie Allen, Jorge
1022 Alvarez-Jarreta, M Ridwan Amode, Irina M Armean, Andrey G Azov, Ruth Bennett, Jyothish
1023 Bhai, Konstantinos Billis, Sanjay Boddu, José Carlos Marugán, Carla Cummins, Claire
1024 Davidson, Kamalkumar Dodiya, Reham Fatima, Astrid Gall, Carlos Garcia Giron, Laurent
1025 Gil, Tiago Grego, Leanne Haggerty, Erin Haskell, Thibaut Hourlier, Osagie G Izuogu, Sophie
1026 H Janacek, Thomas Juettemann, Mike Kay, Ilias Lavidas, Tuan Le, Diana Lemos, Jose
1027 Gonzalez Martinez, Thomas Maurel, Mark McDowall, Aoife McMahon, Shamika Mohanan,
1028 Benjamin Moore, Michael Nuhn, Denye N Oheh, Anne Parker, Andrew Parton, Mateus
1029 Patricio, Manoj Pandian Sakthivel, Ahamed Imran Abdul Salam, Bianca M Schmitt, Helen
1030 Schuilenburg, Dan Sheppard, Mira Sycheva, Marek Szuba, Kieron Taylor, Anja Thormann,
1031 Glen Threadgold, Alessandro Vullo, Brandon Walts, Andrea Winterbottom, Amonida
1032 Zadissa, Marc Chakiachvili, Bethany Flint, Adam Frankish, Sarah E Hunt, Garth IIsley,
1033 Myrto Kostadima, Nick Langridge, Jane E Loveland, Fergal J Martin, Joannella Morales,
1034 Jonathan M Mudge, Matthieu Muffato, Emily Perry, Magali Ruffier, Stephen J Trevanion,
1035 Fiona Cunningham, Kevin L Howe, Daniel R Zerbino, Paul Flicek, Ensembl (2020). *Nucleic*
1036 *Acids Research*, **48**, D1, D682–D688, https://doi.org/10.1093/nar/gkz966

1037 Yoon BS, Ovchinnikov DA, Yoshii I, Mishina Y, Behringer RR, Lyons KM. 2005. Bmpr1a and
1038 Bmpr1b have overlapping functions and are essential for chondrogenesis in vivo. *P Natl Acad*
1039 *Sci Usa* **102**:5062–5067. doi:10.1073/pnas.0500031102

1040 Young NM, Chong HJ, Hu D, Hallgrímsson B, Marcucio RS. 2010. Quantitative analyses link
1041 modulation of sonic hedgehog signaling to continuous variation in facial growth and shape.
1042 *Development* **137**:3405–3409. doi:10.1242/dev.052340

1043 Yue F, Cheng Y, Breschi A, Vierstra J, Wu W, Ryba T, Sandstrom R, Ma Z, Davis C, Pope BD,
1044 Shen Y, Pervouchine DD, Djebali S, Thurman RE, Kaul R, Rynes E, Kirilusha A, Marinov
1045 GK, Williams BA, Trout D, Amrhein H, Fisher-Aylor K, Antoshechkin I, DeSalvo G, See L-
1046 H, Fastuca M, Drenkow J, Zaleski C, Dobin A, Prieto P, Lagarde J, Bussotti G, Tanzer A,
1047 Denas O, Li K, Bender MA, Zhang M, Byron R, Groudine MT, McCleary D, Pham L, Ye Z,
1048 Kuan S, Edsall L, Wu Y-C, Rasmussen MD, Bansal MS, Kellis M, Keller CA, Morrissey CS,
1049 Mishra T, Jain D, Dogan N, Harris RS, Cayting P, Kawli T, Boyle AP, Euskirchen G,
1050 Kundaje A, Lin S, Lin Y, Jansen C, Malladi VS, Cline MS, Erickson DT, Kirkup VM,
1051 Learned K, Sloan CA, Rosenbloom KR, Sousa BL de, Beal K, Pignatelli M, Flicek P, Lian J,
1052 Kahveci T, Lee D, Kent WJ, Santos MR, Herrero J, Notredame C, Johnson A, Vong S, Lee
1053 K, Bates D, Neri F, Diegel M, Canfield T, Sabo PJ, Wilken MS, Reh TA, Giste E, Shafer A,
1054 Kutyavin T, Haugen E, Dunn D, Reynolds AP, Neph S, Humbert R, Hansen RS, Bruijn MD,
1055 Selleri L, Rudensky A, Josefowicz S, Samstein R, Eichler EE, Orkin SH, Levasseur D,
1056 Papayannopoulou T, Chang K-H, Skoultchi A, Gosh S, Disteche C, Treuting P, Wang Y,
1057 Weiss MJ, Blobel GA, Cao X, Zhong S, Wang T, Good PJ, Lowdon RF, Adams LB, Zhou X-
1058 Q, Pazin MJ, Feingold EA, Wold B, Taylor J, Mortazavi A, Weissman SM,
1059 Stamatoyannopoulos JA, Snyder MP, Guigo R, Gingeras TR, Gilbert DM, Hardison RC, Beer
1060 MA, Ren B, Consortium TME. 2014. A comparative encyclopedia of DNA elements in the
1061 mouse genome. *Nature* **515**:355. doi:10.1038/nature13992

1062
1063
1064
1065
1066
1067
1068
1069
1070
1071
1072
1073

Figure 1. Schematic of the many-to-many relationship between genetic and phenotypic variation. From left to right: Allelic variation (colored dots) at individual genes is organized into developmental processes. Processes differ in start/end and duration during development. Genes are reused for different processes at different times. Processes are substantially pleiotropic in their effects contributing to global variation as well as local variation.

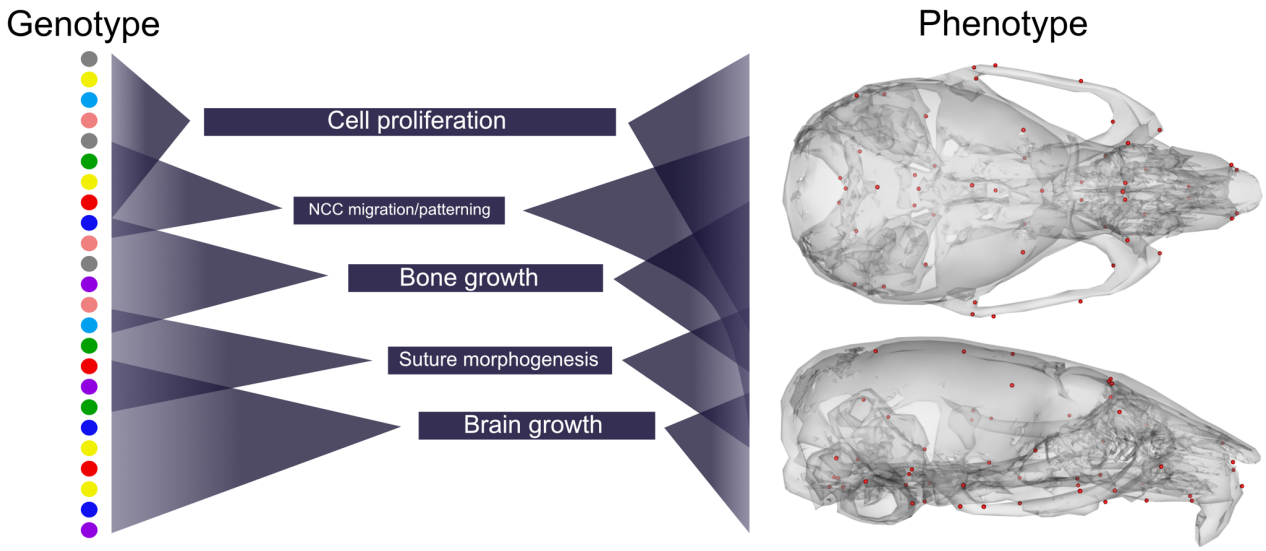

Figure 2. Process MGP for chondrocyte differentiation. A) PLS1 genetic loadings are shown for each gene in the model. Individual founder allele effect sizes are colored within each bar. B-C) Estimated chondrocyte differentiation MGP phenotype is shown with black vectors multiplied 4x. A *Bmpr1b* (*Alk6*) homozygous mutant is shown with red vectors for comparison. The vector correlation between chondrocyte differentiation MGP and *Bmpr1b* is shown below the phenotypic effects.

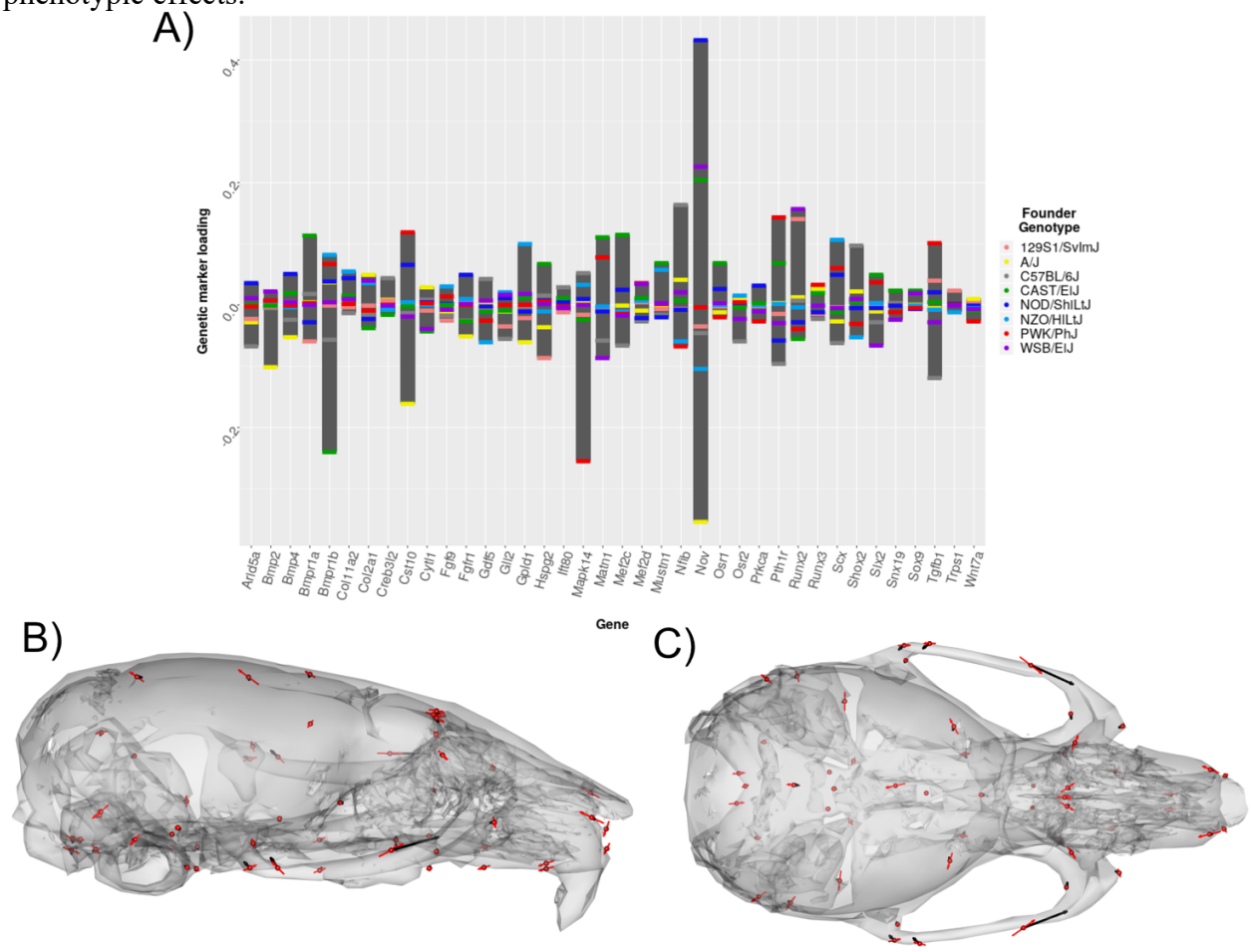

Chondrocyte differentiation map -> Bmpr1b -/-
r = .312

Figure 3. Process MGP for Fgf signaling. A) PLS1 genetic loadings are shown for each gene in the model. Individual founder allele effect sizes are colored within each bar. B-C) Estimated Fgf signaling MGP phenotype is shown with black vectors multiplied 4x. An *Fgf10* homozygous mutant is shown with red vectors for comparison. The vector correlation between Fgf signaling MGP and the *Fgf10* mutant is shown below the phenotypic effects.

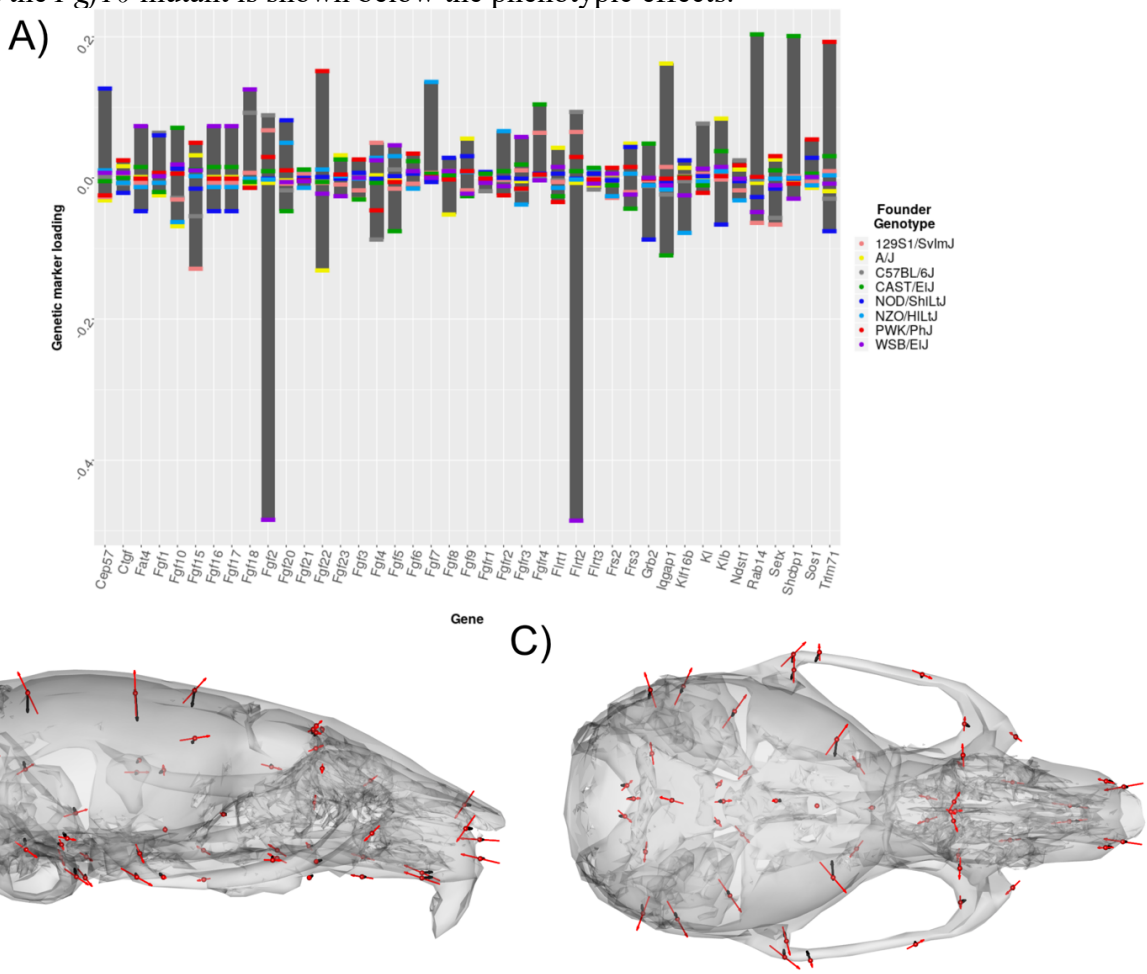

Figure 4. Pairwise MGP vector correlations and random process correlations to principal components. A) Pairwise correlations of phenotypic effects for 15 process MGP analyses. Scale on the right denotes color correspondences to vector correlation, where yellows are high correlations, greens are moderate, and blues are low. B) The densities of vector correlations between 1000 randomly chosen process MGP effects and PCs 1-4.

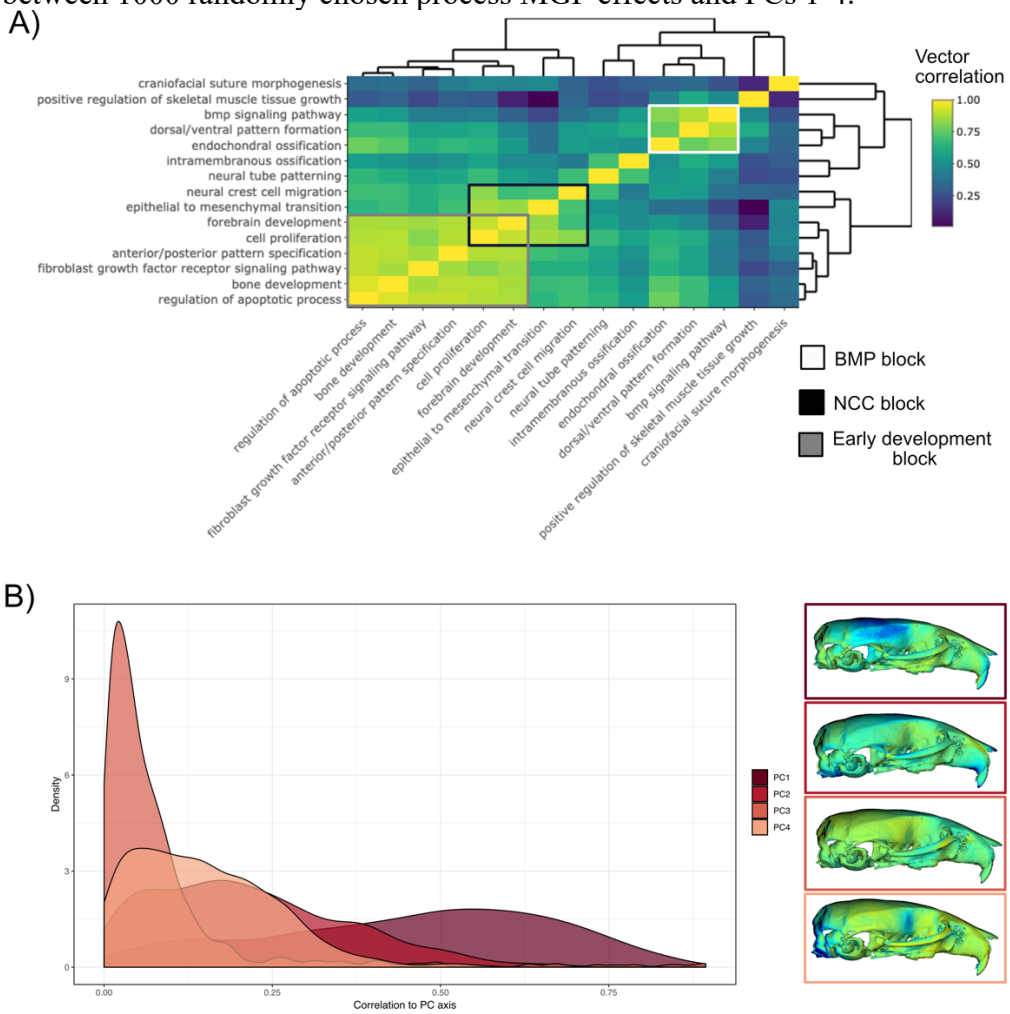

Figure 5. Comparisons of MGP and mouse mutant directions. A) Seven MGP phenotypes projected onto a PCA of the DO and a sample of 30 mutant mouse genotypes. Mutant means are labeled in black. The directions of MGP effects are shown with orange vectors from the DO mean to the associated process MGP. The range of DO variation on PCs 1 and 2 is shown with the shaded ellipse with an orange border. B) A heatmap of vector correlations between 30 mutant effects and 30 process MGP effects.

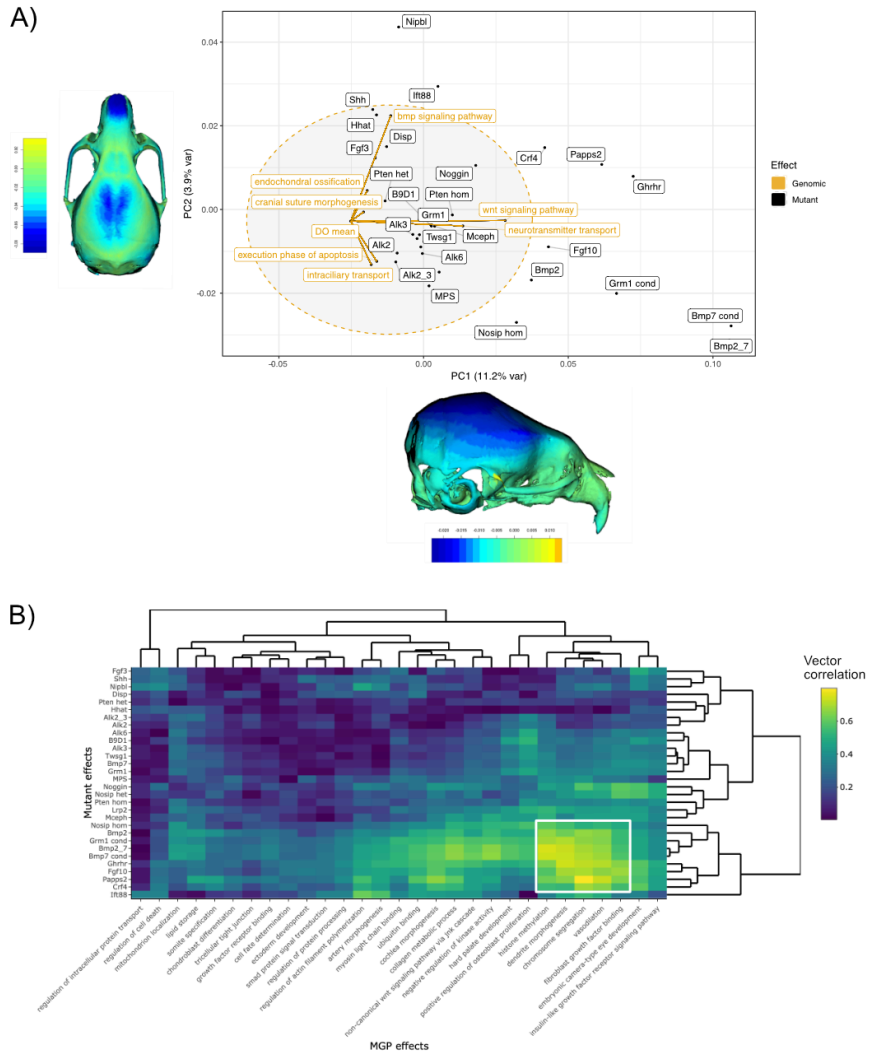

Figure 6. Example screenshot of web version of process analysis. Analyses include a barplot of the relative effect sizes of each selected marker and the associated phenotype shown with black vectors at each landmark. If a mutant comparison is selected, the vector correlation is provided and the mutant phenotype is shown with red vectors. Selecting “send me the results” generates an HTML report with an interactive 3D model.

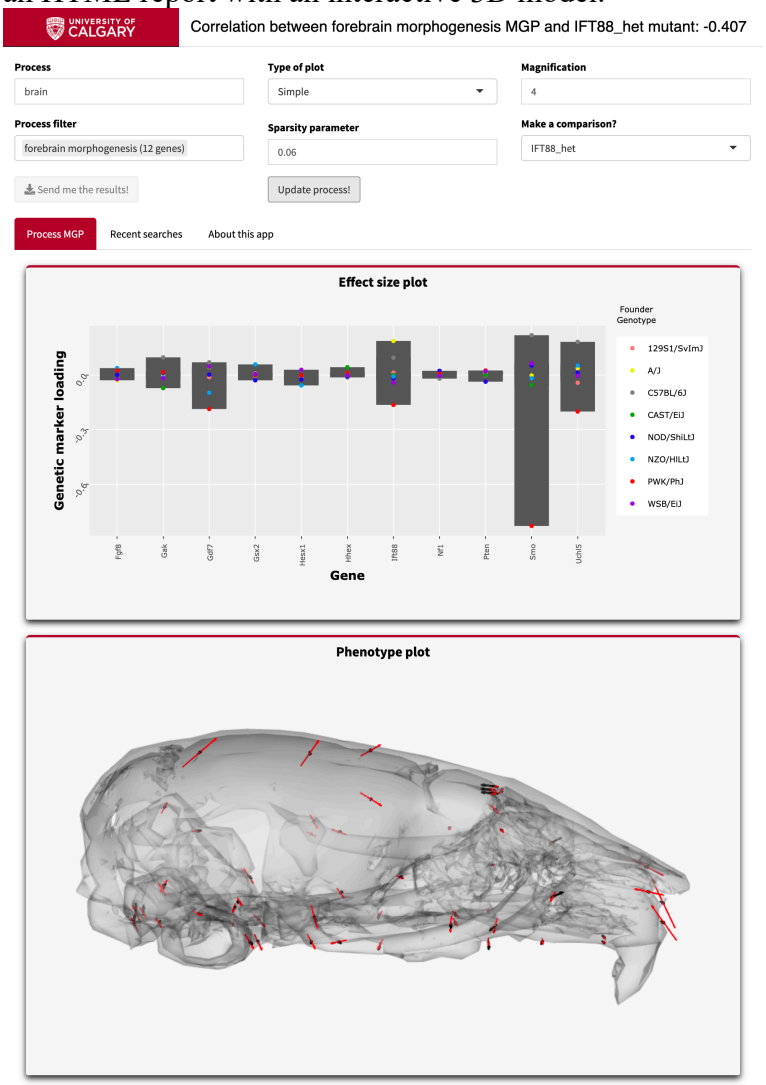

Figure 7. 54 3D landmark configuration. A) Sagittal view of representative scan with landmarks shown as red spheres. B) Dorsal view of landmark configuration. C) Ventral view of landmark configuration.

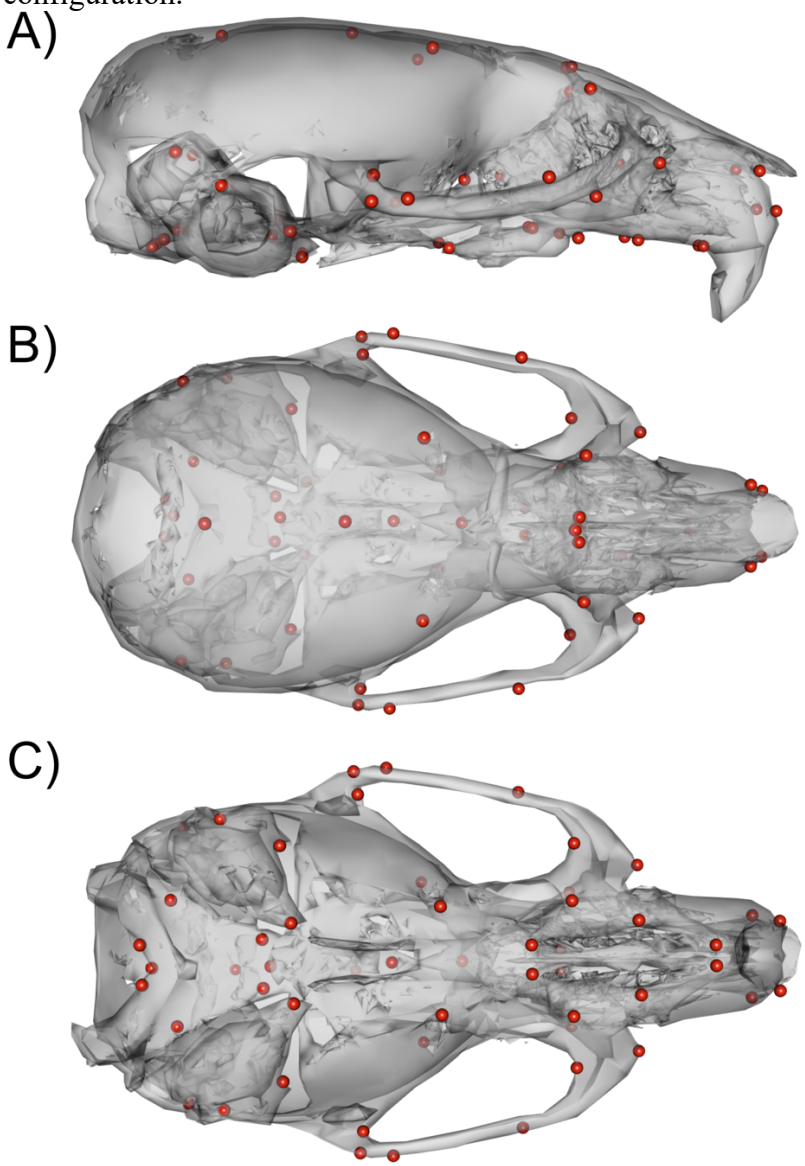

Figure 8. Process MGP schematic. Once a process is selected, we cross-reference the known gene locations with the locations of the genotyped markers in the DO sample. The founder probabilities of the nearest upstream and downstream markers are averaged for each gene. The compiled founder probabilities and landmark coordinates are then used in a regularized PLS model to estimate latent axes of covariation.

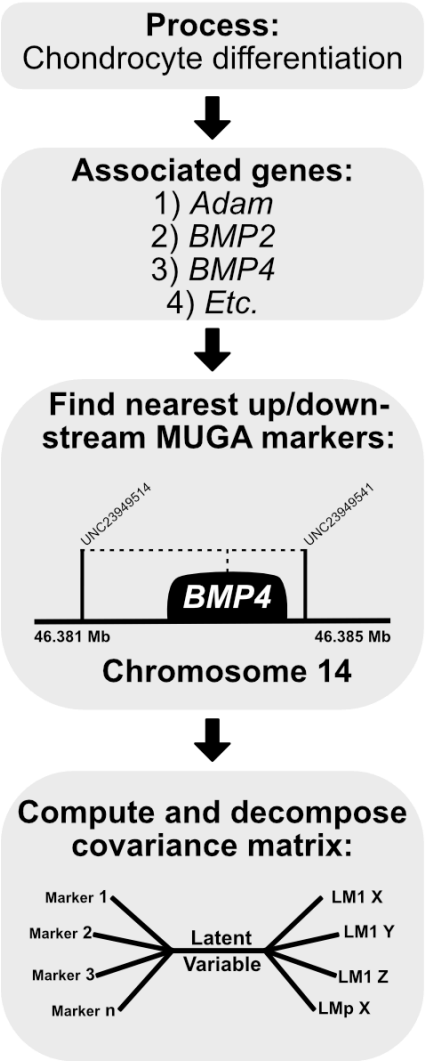

1227 Supplemental figure 1. Permutation of marker sets of fixed size. A) The permuted R^2 distribution
1228 of 1000 38-marker MGP analyses is shown in blue. The estimated R^2 of the chondrocyte
1229 differentiation MGP is shown as a black vertical line. B) The permuted R^2 distribution of 1000
1230 41-marker MGP analyses is shown in blue. The estimated R^2 of the Fgf signaling MGP is shown
1231 as a black vertical line.
1232

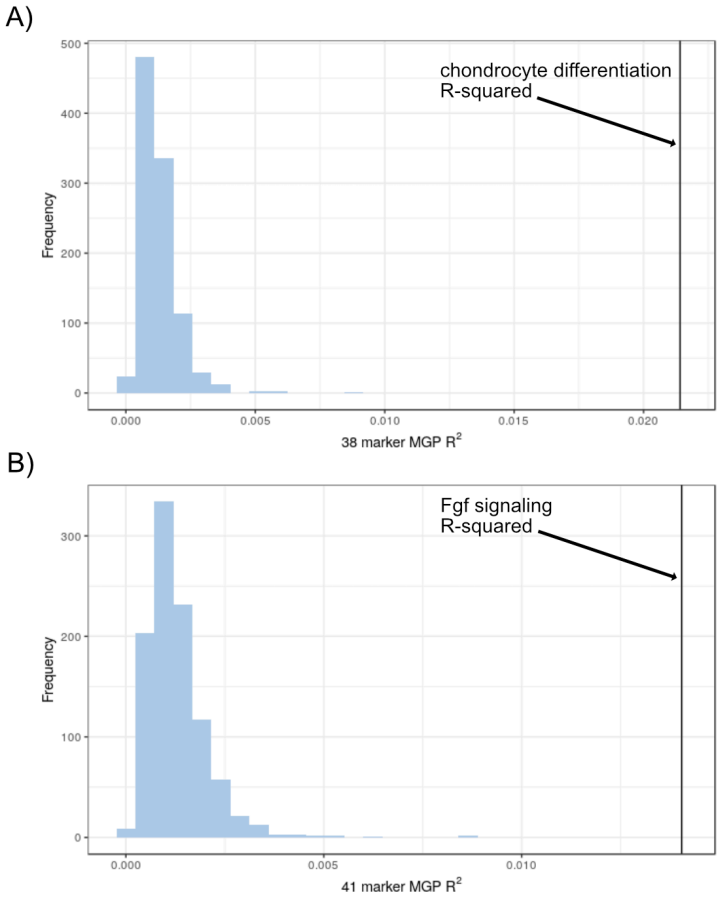

1233
1234
1235
1236
1237
1238
1239
1240
1241
1242
1243
1244
1245
1246
1247
1248

Supplemental figure 2. Genetic effect loadings for multiple process MGPs. Selected processes are listed above their respective plots. Marker loadings are not scaled to a common range.

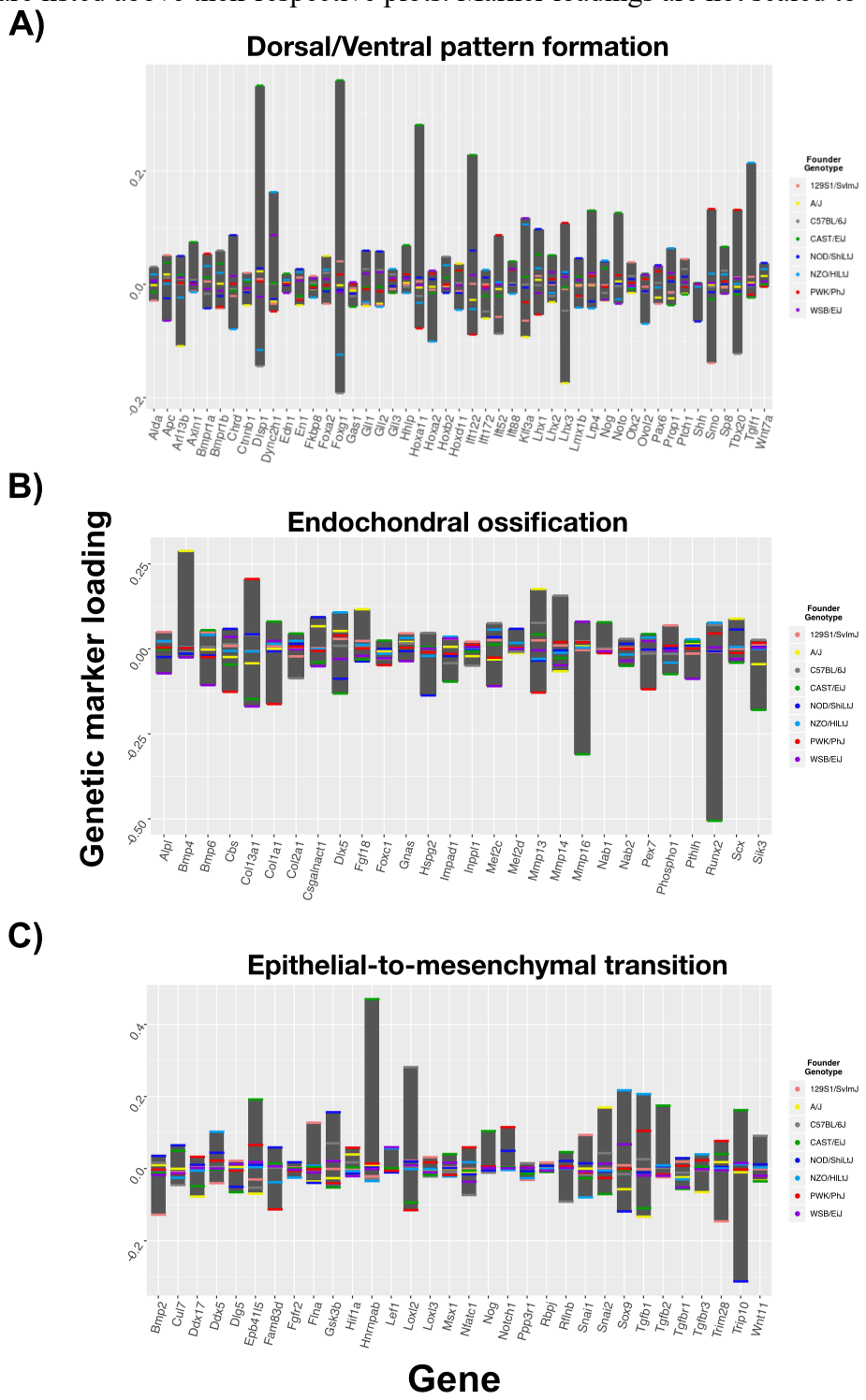

Supplemental figure 3. Additional process-to-mutant comparisons. A) The estimated chondrocyte differentiation MGP phenotype magnified 4x (black) with *Bmp2* homozygous mutant (red). B) The estimated Fgf signaling MGP phenotype magnified 4x (black) with *Fgf3* homozygous mutant (red).

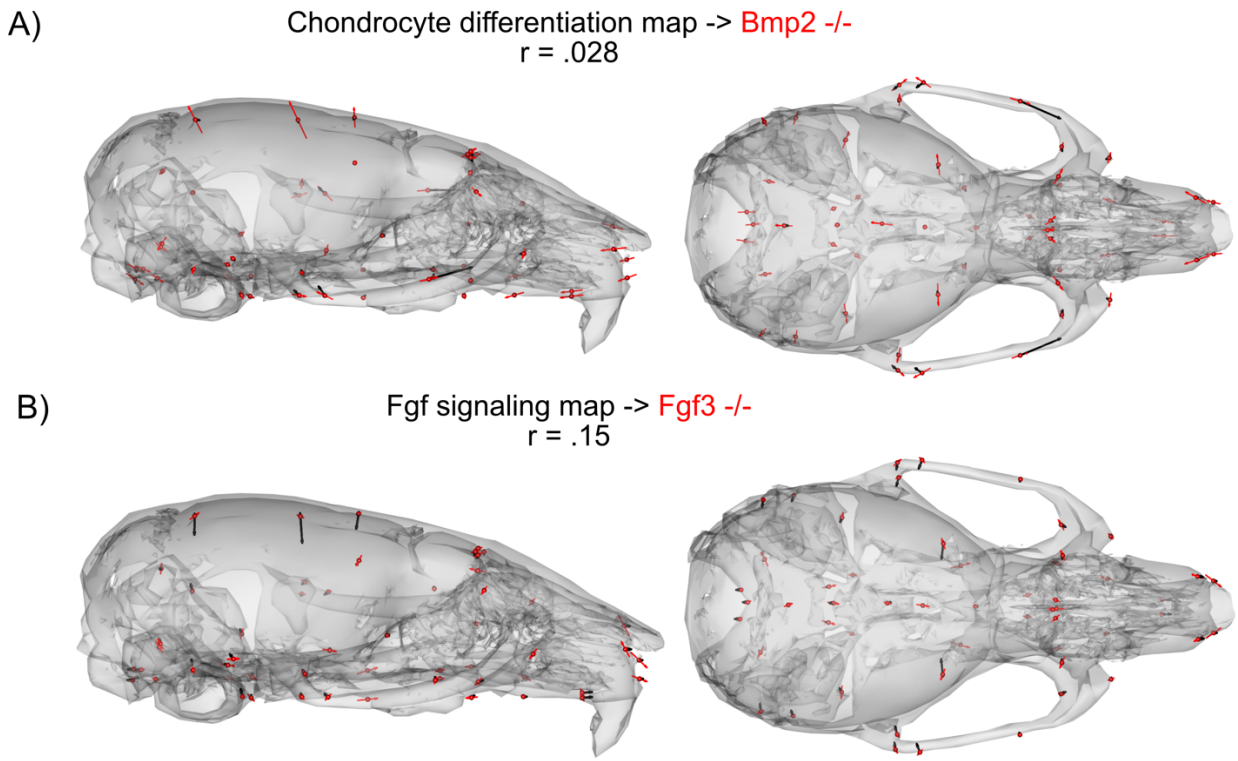

Supplemental figure 4. Demographic plots for the DO sample. A) The distribution of the sample by generation and data source (lab). B) Distribution of sex by source (lab).

A)

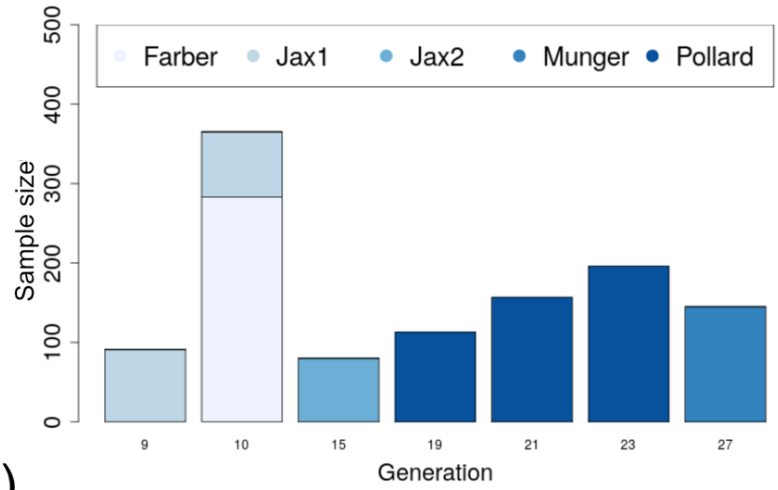

B)

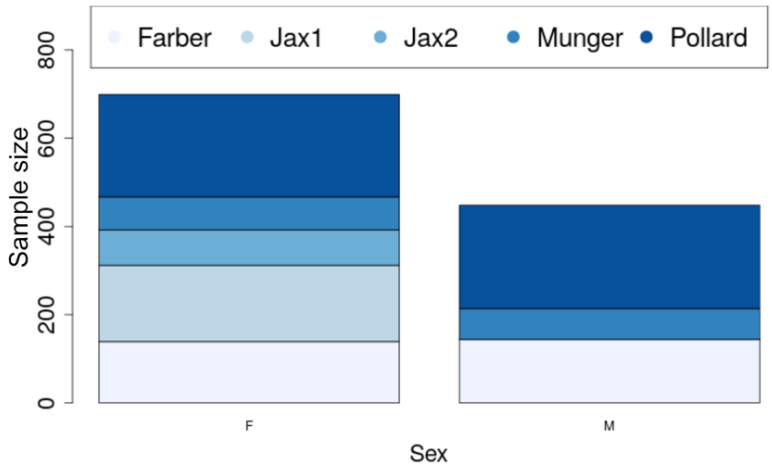

Supplemental figure 5. Histogram of kinship matrix values in the DO sample.

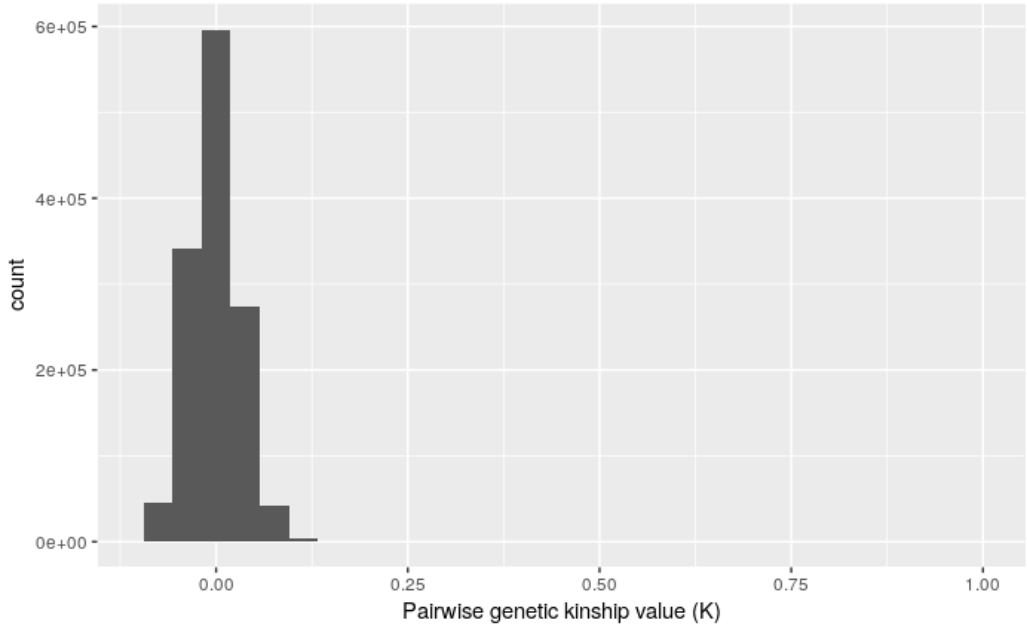

Supplemental figure 6. Combining queries in the MGP shiny app with the pipe operator. In order to filter the GO database with multiple terms, the pipe operator can be used as shown. Here, the user has selected processes associated with either the apoptosis or Wnt pathway process. The barplot shows the relative effect sizes for markers associated to both “Wnt signaling pathway” and “execution phase of apoptosis” GO terms.

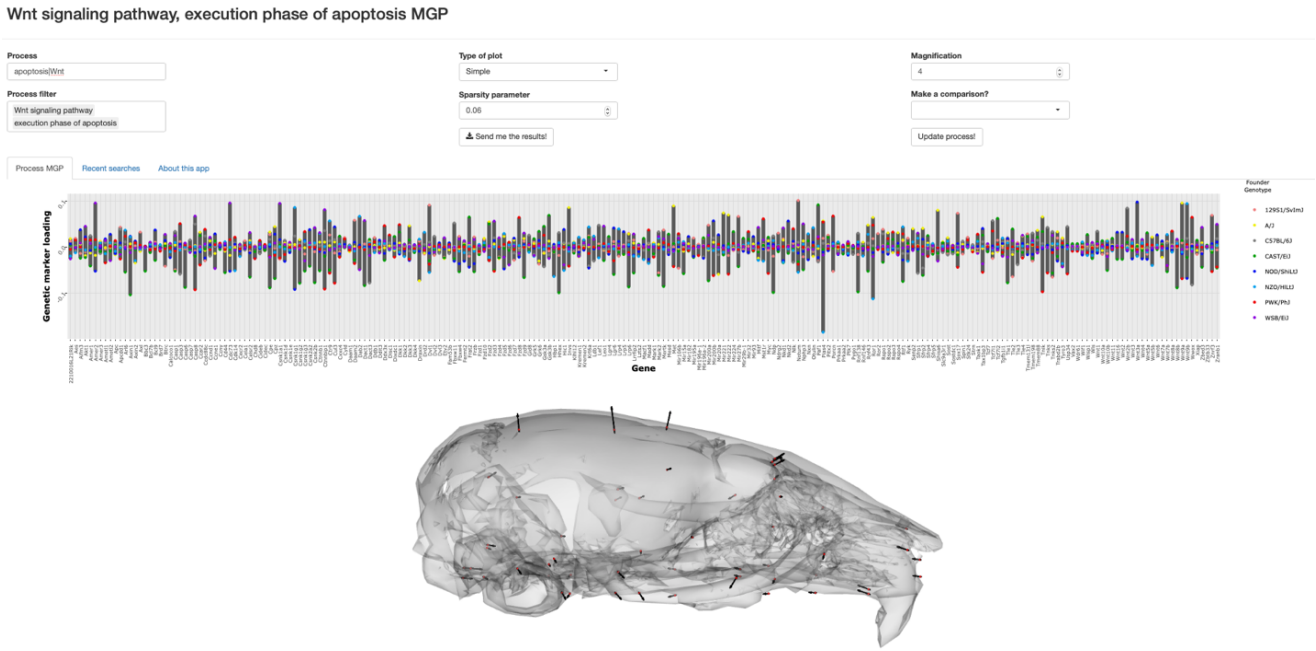

1354 Supplemental table 1. Top 10 MGP vector correlations with PC1. Corresponding PC2- 4 vector
1355 correlations are also provided.

PROCESS	PC1 CORRELATION	PC2 CORRELATION	PC3 CORRELATION	PC4 CORRELATION
ZINC ION BINDING	0.859241	0.01277426	0.07172876	0.20641736
SENSORY PERCEPTION OF SOUND	0.84834632	0.10996389	0.0407517	0.20432551
CALCIUM ION TRANSPORT	0.84816486	0.16123711	0.05231719	0.11159004
PROTEIN HOMOOLIGOMERIZATION	0.84782484	0.20793974	0.0156349	0.16244344
DENDRITE MORPHOGENESIS	0.84752457	0.06832718	0.10026087	0.07711775
NEUROPEPTIDE SIGNALING PATHWAY	0.84620616	0.21526031	0.02883174	0.13173442
FOCAL ADHESION	0.84611744	0.13458614	0.04380431	0.21903587
CHROMOSOME SEGREGATION	0.84610062	0.10383492	0.03360725	0.16218602
SARCOMERE ORGANIZATION	0.83893574	0.15368816	0.02581707	0.02880551
INTEGRAL COMPONENT OF ENDOPLASMIC RETICULUM MEMBRANE	0.83775207	0.1673053	0.03517157	0.02691882

1356
1357
1358 Supplemental table 2. Processes with moderate vector correlations to PC 1-4.

PROCESS	PC1 CORRELATION	PC2 CORRELATION	PC3 CORRELATION	PC4 CORRELATION
NEGATIVE REGULATION OF I-KAPPAB KINASE/NF-KAPPAB SIGNALING	0.54158492	0.25581449	0.49244383	0.25894853
LOCOMOTORY EXPLORATION BEHAVIOR	0.37993095	0.2110723	0.68937988	0.24189284
AU-RICH ELEMENT BINDING	0.57006676	0.32997589	0.40318313	0.20843601
TRANSCRIPTION REGULATORY REGION SEQUENCE-SPECIFIC DNA BINDING	0.70056311	0.09294266	0.44398467	0.26285711
DYNEIN COMPLEX	0.68525872	0.24644459	0.31380962	0.19363051
PRESYNAPTIC CYTOSOL	0.39216186	0.38329479	0.13557636	0.50766778
NEGATIVE REGULATION OF FAT CELL DIFFERENTIATION	0.39080052	0.24460715	0.73049567	0.02976212
CELL BODY	0.80176806	0.25146354	0.06871634	0.2628449
ADULT BEHAVIOR	0.74617475	0.3923876	0.03450902	0.21024944
PROTEASOMAL UBIQUITIN-INDEPENDENT PROTEIN CATABOLIC PROCESS	0.61654501	0.39974619	0.09993121	0.26252902

1359
1360
1361
1362
1363